Analysing Vascular Structure for Detection of IntraRetinal MicroVascular Abnormalities (IRMA)

Author

Rabeeah Ali

NUST201464491MCEME35214F

Supervisor

Dr. Muhammad Usman Akram

DEPARTMENT OF COMPUTER ENGINEERING

COLLEGE OF ELECTRICAL & MECHANICAL ENGINEERING

NATIONAL UNIVERSITY OF SCIENCES AND TECHNOLOGY

ISLAMABAD

AUGUST, 2018

Analysing Vascular structure for detection of IntraRetinal MicroVascular Abnormalities (IRMA)

Author

Rabeeah Ali

NUST201464491MCEME35214F

A thesis submitted in partial fulfillment of the requirements for the degree of

MS Computer Engineering

Thesis Supervisor

Dr. Muhammad Usman Akram

Thesis Supervisor's Signature: _____

DEPARTMENT OF COMPUTER ENGINEERING

COLLEGE OF ELECTRICAL & MECHANICAL ENGINEERING

NATIONAL UNIVERSITY OF SCIENCES AND TECHNOLOGY,

ISLAMABAD

AUGUST- 2018

Declaration

I certify that this research work titled "*Analysing Vascular structure for detection of IntraRetinal MicroVascular Abnormalities (IRMA)* is my own work. The work has not been presented elsewhere for assessment. The material that has been used from other sources it has been properly acknowledged / referred.

Signature of Student

Rabeeah Ali

NUST201464491MCEME35214F

Language Correctness Certificate

This thesis has been read by an English expert and is free of typing, syntax, semantic, grammatical and spelling mistakes. Thesis is also according to the format given by the university.

Signature of Student

Rabeeah Ali
NUST201464491MCEME35214F

Signature of Supervisor

Dr.Muhammad Usman Akram

Copyright Statement

Acknowledgements

In the name of Allah, the most gracious, the most merciful. It is surely due to His will that my thesis has reached its final stage, for anything sans His orders cannot exist. I am thankful for all the courage, knowledge and ability He gave me to go on with the work despite all the circumstances and for the patience He instilled in those around me to help me with it.

In this context, I would like to express sincere gratitude to my advisor Dr. Muhammad Usman Akram for boosting my morale and for his continual dedication, assistance and motivation. He is one of the few people, I have seen, who are honest to their work. I am blessed to have such a co-operative advisor and kind mentor for my research.

Along with my advisor, I would like to acknowledge my entire thesis committee: Dr. Arsalan Shaukat and Dr. Shoab Ahmed Khan for their cooperation and suggestions.

I am profusely thankful to my whole family for all the physical and moral support they have provided: my beloved Parents and sisters, in-laws specially my mother in law and sister in law, my husband and children who were there with me through all the thick and thin.

A special note of thanks to Dr. Qamar Farooq, Head of Department Ophthalmology, Rawalpindi Medical College (RMC) and Dr. Assu Kumar, an eye specialist in Saudi Arabia for their valuable input in dataset annotation.

Last but not the least, I am grateful to my friends and classmates for their well wishes and motivation.

Dedicated to my parents: ***Dr. Ali Bakhteyar & Dr. Mehr Jabeen, Mr. Shamim, and Mrs. Zeba Shamim****, and husband,* ***Mr.Waqqas*** *whose tremendous support and cooperation led me to this accomplishment.*

Abstract

Retinal fundus images are coloured images obtained through specially designed cameras through a dilated pupil of the patient. Analysis of these images is being used to detect retinal vascular abnormalities to provide insight into onset or severity of retinopathies specially hypertensive or diabetic retinopathy. One of the common yet significant change that occurs is the change in vascular shape; in that the vessel(s) becomes non-periodically twisted; more generally termed as an increase in tortuosity. This thesis presents a simple and reasonably accurate algorithm to classify a vessel as tortuous or not, through determining a set of features. A new set of features is proposed in this research for reliable detection of vascular changes. The proposed method uses One Class SVM (OC-SVM), commonly used for anomaly detection. The reason for using OC-SVM is that the ratio of tortuous vessels as compared to normal ones is very low and they mostly appear as anomaly when compared with normal vessels. A local dataset of 100 fundus images is used for evaluation. The dataset has manually extracted vessels, veins and arteries as ground truth and also contains annotation with respect to vessel tortuosity. The experiments are conducted by randomly dividing data into 60 per cent for training and 40 per cent for testing. The experiments are repeated 10 times and average results are reported. The results show that the proposed system provides an efficient non-invasive technique to detect tortuous vessels and an important step towards detecting IRMA.

Key Words: *diabetic, retinopathy, vessel, tortuosity, medical image processing, IRMA, One Class SVM*

Table of Contents

DECLARATION ..... **I**
LANGUAGE CORRECTNESS CERTIFICATE ..... **II**
COPYRIGHT STATEMENT ..... **III**
ACKNOWLEDGEMENTS ..... **IV**
ABSTRACT ..... **VII**
TABLE OF CONTENTS ..... **VIII**
TABLE OF FIGURES ..... **IX**
1. INTRODUCTION **11**
1.1. MOTIVATION 11
1.2. PROBLEM STATEMENT 12
1.3. AIMS AND OBJECTIVES 12
1.4. STRUCTURE OF THESIS 12
2. CLINICAL PERSPECTIVE OF DIABETIC RETINOPATHY **13**
2.1. OCULAR ANATOMY 13
2.2. DIABETES MELLITUS (DM) 13
2.3. DIABETIC RETINOPATHY (DR) 14
2.3.1. Non-proliferative Diabetic Retinopathy (NPDR) *16*
2.3.2. Proliferative Diabetic Retinopathy (PDR) *20*
2.4. TORTUOSITY 21
3. LITERATURE REVIEW **23**
3.1. DISTANCE BASED TECHNIQUES: 24
3.2. CURVATURE BASED TECHNIQUES 24
3.3. HYBRID TECHNIQUES 28
4. METHODOLOGY **33**
4.1. SEGMENTATION 34
4.1.1. Background Noise Removal *35*
4.1.2. Vessel Segmentation *37*
4.1.3. Skelotonisation and Bifurcation points *43*
4.1.4. Seperated Vessel Segments *45*
4.1.5. Feature Extraction *45*
Structure based features *45*
Peak based features *47*
Gradient based features *47*
4.2. CLASSIFICATION 49
One Class Support Vector Machines *49*
5. EXPERIMENTAL RESULTS **53**
5.1 DATASET AND SPECIFICATIONS 53
5.2 PERFORMANCE MEASURES 58
5.3 RESULTS 58
6. CONCLUSION AND FUTURE WORK **68**
6.1 CONCLUSION 68
6.2 CONTRIBUTION 68
6.3 FUTURE WORK 68
REFERENCES **69**

Table of figures

FIGURE 2-1 RETINAL FUNDUS IMAGING [4] 13
FIGURE 2-2 ANATOMICAL DIAGRAM OF AN EYE [5] 13
FIGURE 2-3 FUNDUS IMAGE OF: (A) A HEALTHY NORMAL RETINA (B) DISEASED RETINA SHOWING A COMBINATION OF DR SYMPTOMS [7] 15
FIGURE 2-4 (A) MICROANEURYSM (MA) (B) FFA IMAGE OF MA [7] 16
FIGURE 2-5 FUNDUS IMAGE SHOWING (A) NORMAL VASCULAR NETWORK (B) VENOUS TORTUOSITY 17
FIGURE 2-6 DOT AND BLOT INTRA-RETINAL HEMORRHAGES, NOTICE THE DOT LIKE APPEARANCE IN LEFT FIGURE AND A BLOT IN THE RIGHT ONE [7] ... 17
FIGURE 2-7(A) FLAME HEMORRHAGE (B) A REPRESENTATION OF HOW A FLAME APPEARS IN THE RETINAL LAYERS [7] 18
FIGURE 2-8 LIPID EXUDATES AS A RESULT OF MACULAR EDEMA [9] 18
FIGURE 2-9 COTTON WOOL LESIONS IN POSTERIOR EYE [9] 18
FIGURE 2-10 SIGNIFICANTLY TORTUOUS BLOOD VESSEL 18
FIGURE 2-11: (A) VENOUS LOOPING (OMEGAS) (B) VENOUS BEADING NOTICE THE DILATION AND THINNING [8] 19
FIGURE 2-12(A)MAGNIFIED IMAGE SHOWING IRMA (B) A VERY CLEAR SHUNT VESSEL DEVELOPED DUE TO IRMA [10] 20
FIGURE 2-13 NVD 21
FIGURE 2-14 NVE 21
FIGURE 2-15 NORMAL VASCULAR NETWORK 22
FIGURE 2-16 VENOUS TORTUOSITY 22
FIGURE 2-17 MAGNIFIED IMAGE SHOWING IRMA 22
FIGURE 3-1 ARC TO LENGTH RATIO OF TWO DIFFERENT CURVES 24
FIGURE 3-2 CURVATURE CALCULATION USING A CIRCULAR MASK 25
FIGURE 3-3 RESULT OF HOUGH TRANSFORM, ONLY TWO CONCENTRIC CIRCLES (WITH CENTER ‘C’) WITH CLOSE RADIUS, ARE POSITIONED CORRECTLY ON A CURVE 26
FIGURE 3-4 CURVATURE CALCULATION WITH THE TEMPLATE DISK METHOD 27
FIGURE 3-5 APPROXIMATING AREA A USING CROSSOVER OF CURVE AND TEMPLATE DISK 28
FIGURE 3-6 ANGLE MEASURED BETWEEN THE ANGULAR BISECTOR NEAR THE END OF A CURVE. 29
FIGURE 3-7 FILTER MASK AND ITS MOVEMENT 30
FIGURE 3-8 SUPERIMPOSING CIRCLES OF EQUAL RADII TO TRAVERSE THE CURVE 31
FIGURE 4-1 FLOW CHART OF METHODOLOGY (SKELOTONISED IMAGE IS SHOWN IN WHITE BACKGROUND FOR CLARITY) 34
FIGURE 4-2 STEPS TO REMOVE ANY BACKGROUND NOISE (A) COLORED INPUT IMAGE B) THREHSOLDING (C)IMAGE AFTER APPLYING THE MEDIAN FILTER (D) REMOVING SMALL SPURS AND FILLING IN HOLES (IF ANY) (E)MINOR EROSION WITH A DISK OF RADIUS 5 (F) RESULTANT MASK 35
FIGURE 4-3 PROBING OF AN IMAGE USING A SQUARE STRUCTURING ELEMENT [26] 36
FIGURE 4-4 FLOW CHART OF VESSEL NETWORK EXTRACTION 38

FIGURE 4-5 (A) RGB FUNDUS IMAGE (B) GREEN CHANNEL (C) INVERTED GREEN CHANNEL 38
FIGURE 4-6 : (A) ORIGINAL IMAGE (B) CENTERED FREQUENCY RESPONSE (C) INVERSE FFT.....39
FIGURE 4-7 GABOR WAVELET WITH A=2, X_0=0 AND K_0 =1 40
FIGURE 4-8 WAVELET ORIENTATIONS AND RESPONSES (A) FFT GABOR WAVELET ORIENTATION (B)CENTERED FFT RESPONSE (C) FFT RESULT OF CORRELATION WITH THE IMAGE (D) RESULTS IN THE SPATIAL DOMAIN .41
FIGURE 4-9 (A) THE GREEN INVERTED IMAGE (B) WAVELET BASED ENHANCED VASCULAR TREE (C) SEPARATED VASCULAR NETWORK.....42
FIGURE 4-10 (A) REMOVING THE CIRCULAR BOUNDARY (B) MORPHOLOGICAL CLOSING (C) REMOVING SMALL SPUR.....42
FIGURE 4-11 (A) GREEN CHANNEL IMAGE (B) WAVELET VESSEL ENHANCEMENT (C) EXTRACTED VESSEL TREE 43
FIGURE 4-12 SKELOTONISATION (A) ORIGINAL VESSEL MASK (B) AFTER 2 ITERATIONS (C) AFTER 5 ITERATIONS (D) VESSEL SKELETON.....44
FIGURE 4-13 BRANCH POINTS ON THE VESSEL TREE MARKED WITH RED-CROSS.....44
FIGURE 4-14 LABELLED VESSEL SEGMENTS SHOWN IN DIFFERENT COLORS ...45
FIGURE 4-15 VASCULAR SEGMENTS WITH DIFFERENT TORTUOSITY 46
FIGURE 4-16 (A)PEAKS DETECTED FOR EACH VASCULAR SEGMENT MARKED WITH RED CIRCLES (B) PEAK WIDTH (YELLOW HORIZONTAL LINE) AND PEAK PROMINENCE (RED VERTICAL LINE).....47
FIGURE 4-17 (A) SHOWS THE GRADIENT MAGNITUDE (L) AND DIRECTION IMAGES (R), (B) ARROWS SHOWING THE MAGNITUDE AND DIRECTION OF VESSEL SEGMENTS.....48
FIGURE 4-18 LINEAR SVM MODEL FOR TWO CLASSES- THE CHOSEN HYPER-PLANE GIVES THE MAXIMUM DISTANCE BETWEEN THE TWO CLASSES. POINTS LYING ON THE DOTTED LINES ARE CALLED SUPPORT VECTORS [16].....50
FIGURE 4-19 HYPER-PLANE EXAMPLES FOR DIFFERENT DATA SCENARIOS IN SVM [29] 51
FIGURE 4-20 ONE CLASS SVM MODEL 52
FIGURE 5-1 IMAGES FROM LOCAL DATASET, [3RD ROW] SHOWS ARTERIES (RED) AND VEINS (BLUE) 53
FIGURE 5-2 SCATTER PLOT OF FEATURES (XVARS VS YVARS), CROSS= CLASS 0 (TORTUOUS VESSELS), SQUARE = CLASS 1(NORMAL VESSELS) 56
FIGURE 5-3 SCATTER PLOTS SHOWING DISTRIBUTION OF SAMPLES FOR ARTERIES AND VEINS (XVAR VS YVAR), CROSS = CLASS 0 (TORTUOUS VESSELS), SQUARE = CLASS 1(NORMAL VESSELS).....57
FIGURE 5-4 CONTOUR PLOTS SHOWING SVM BOUNDARY 64
FIGURE 5-5 RECEIVER OPERATING CURVES (ROC) FOR THE THREE FEATURE CATEGORIES, FOR EACH VESSEL TYPE. 65
FIGURE 5-6: ROC CURVES FOR 6 RANDOM ITERATIONS FOR COMBINED VESSELS, ARTERIES AND VEINS 66
FIGURE 5-7 PREDICTED LABELLED VESSELS, LIGHT BLUE = TORTUOUS VESSELS, DARK BLUE = NORMAL VESSELS 67

1. Introduction

Automation is the word of the era. Computers are being used increasingly in all fields of life to assist humans and shorten the time required to complete any process. One such major turning point of technology in health care is Computer Aided Diagnosis (CAD) system. CAD is the use of built in knowledge in computers to mimic a doctor's diagnosis of a medical image. The machine produced diagnosis is usually based on a model derived from earlier observations which helps with the accuracy of the findings. Further advancements include the machine being able to give a diagnosis for a new case that has similar symptoms, precisely known as Artificial Intelligence (AI). Since the introduction of AI, CAD results are being counted as "second opinion" by specialists. One such application of CAD is in detecting retinopathy using ocular fundus images. The blood vessels of the eye are arranged in a unique pattern (creating a vascular network). Various factors such as aging, air pollution and presence of a disease (e.g. hypertension, diabetes and cardiovascular diseases) cause a change in the vascular arrangements and lead to defects that can affect the eyesight and hence hamper vision. These vascular anomalies, generally termed as Intra-retinal Micro-vascular Abnormalities (IRMA) present as changes in the shape of the vessels (tortuous vessels), hemorrhages (blood leakage from the vessels) or blocked blood vessels. Analysis of fundus images is being used to detect these deformities to provide insight into onset or severity of retinopathies specially hypertensive or diabetic retinopathy. The basis of this research is to detect tortuous vessels in fundus images which is an early indicator of IRMA.

1.1. Motivation

Diabetes Mellitus (DM) is a preventable disease and can be treated if diagnosed timely. According to World Health Organization (WHO) the number of people with DM have risen from 108 million in 1980 to 422 million in 2014 [1]. Among other complications, Diabetes is a major cause of Diabetic retinopathy (DR). Currently DR is the leading cause of blindness in working age population and the number of people with DR is expected to grow from 126.6 million in 2010 to an overwhelming figure of 191.0 million by 2030 [2]. DR is more of a problem in developing countries and for the low-income class because (among other factors) tertiary care

eye health centers are not accessible or are too expensive. As timely diagnosis and treatment of DR can stop the disease progression it is vital to develop systems that are reliable and can detect it in early stages.

1.2. Problem Statement

In addition to a healthy lifestyle and proper diet, proper ophthalmological health care in terms of automated systems are required to facilitate eye image analysis. This in turn will help ensure early diagnosis of DR. One of its initial detectable symptoms is the change in retinal vascular tortuosity which is attributed to the stretching of blood vessels due to increase in blood pressure of weak vessel walls [3]. Multiple methods have been proposed to quantify tortuosity but all are computationally heavy due to the intensive mathematical calculations. This thesis presents a simple yet efficient system for detecting tortuous vessels to detect IRMA in a retinal fundus image.

1.3. Aims and Objectives

Major objectives of the research are as follow:

- Collection of annotated dataset for vascular structure analysis
- Review of the state of the art techniques proposed and used to calculate retinal vascular tortuosity
- Formulation of feature set for appropriate representation of tortuous vessels.
- Classification of eye vessel segments and the whole image as tortuous or non-tortuous

1.4. Structure of Thesis

This work is structured as follows:

Chapter 2 describes the general anatomy of an eye, its functioning and a clinical overview of Diabetes and how it affects the eye.
Chapter 3 presents the literature review and the ongoing work on retinal vascular tortuosity
Chapter 4 explains the methodology in detail.
Chapter 5 discusses the results and findings with the aid of figures
Chapter 6 conclusion and future work

2. Clinical Perspective of Diabetic Retinopathy

2.1. Ocular Anatomy

Human eye is the organ that allows vision. It has photoreceptor cells that convert light reflected from objects in to electrical signals to form an image. The photoreceptor cells (rods and cones) are present on the retina- the inner eye layer (shown in figure 2-1) where images are formed.

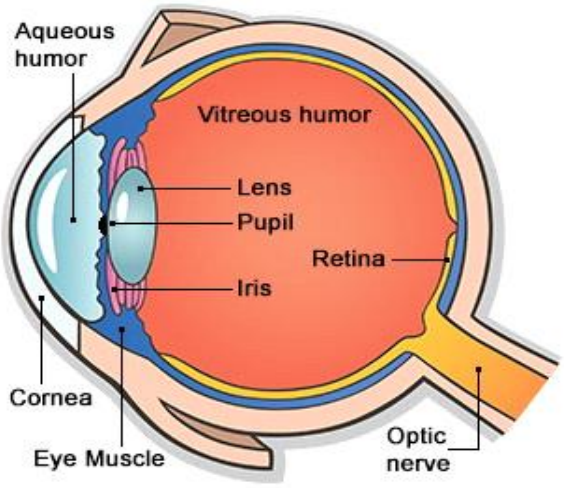

Figure 2-1 Retinal fundus imaging [4]

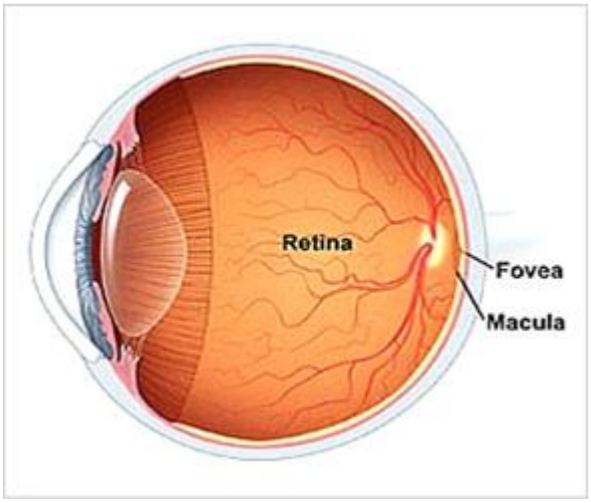

Figure 2-2 Anatomical diagram of an eye [5]

In addition to the rods and cones that help form images, the retina (figure 2-2) has a network of blood vessels that circulates blood to the retina and hence maintains the blood supply in the eye. For each individual these blood vessels are arranged in a unique pattern. Various factors such as aging, air pollution and diseases that include but are not limited to hypertension, diabetes cause a change in the vascular arrangements and lead to abnormalities that can affect the eyesight leading to vision loss or even blindness.

2.2. Diabetes Mellitus (DM)

When we eat, the food is broken down in to smaller units called glucose that can be utilized by our body cells to maintain their growth and metabolism. A hormone called insulin that is released by our pancreas is responsible to regulate the blood glucose levels and allow the cells to uptake it from the blood for utilization and storage.

A disorder of this whole mechanism can cause severe problems.

Diabetes or diabetes mellitus is the medical term used to describe hyperglycemia (high sugar levels) in the blood over a long time period that occurs because the body is unable to regulate the glucose levels in the blood either because the body cannot produce insulin, or the cells are unable to use it or both [6].

There are three types of diabetes:

Type-1: also known as the juvenile or early onset diabetes referring to the inability of the body to produce insulin. Hence it can affect individuals of any age.

Type-2: which occurs due to the fact that the cells are unable to use the insulin. This is the most common type of diabetes. From all the diabetes cases, approximately 90% are type-2 diabetes. Aging and unhealthy lifestyle can increase the risk of type 2 diabetes.

Gestational diabetes: that occurs in expecting mothers due to unhealthy eating habits or hormonal imbalances. It may also increase the risk of developing type-2 diabetes in such individuals.

All types of diabetes are curable or the patient can at least function normally if they take care of their diet and medicines. On the other hand badly controlled diabetes can cause multiple complications in all the organs in the body including the brain, heart, kidneys, lower legs and eye. In fact, diabetes is termed to be the leading cause of ophthalmological diseases where diabetic retinopathy tops the list.

2.3. Diabetic Retinopathy (DR)

As the name suggests, Diabetic retinopathy refers to the progressive damage to the retina that occurs due to uncontrolled diabetes (Retinopathy: diseases of the retina (figure 2-3(b)), Diabetic: due to high sugar levels).

The retina is one of the most fundamental structures of the eye in that it contains all the vessels that maintain oxygen and nutrition supply to the eye. High sugar levels can cause damage to the vascular structure both at macro and the micro level depending on the severity of the disease.

Genetic disposition, age and the duration for which a patient has been diabetic play a significant role in determining the level of retinopathy.

Studies in UK show that DR is the leading cause of preventable blindness in working class individuals [7] where 25% to 33% of diabetic patients also suffer from DR

DR progresses through a series of stages before it causes irreversible damage to the retinal vascular structure. Hence, like most diseases, duration is a primary risk factor, the earlier it is diagnosed and treated, the better the chances for cure.

Figure 2-3 shows a pictorial comparison of (a) a healthy retina with normal blood vessels and (b) diseased retina with multiple complications due to DR.

DR can be classified in to two types:

Non-proliferative Diabetic Retinopathy (NPDR)

Proliferative Diabetic Retinopathy (PDR)

The main differentiating factor between the two is if there is an increase in number of vessels (proliferation) or not for reasons explained below.

(a) (b)

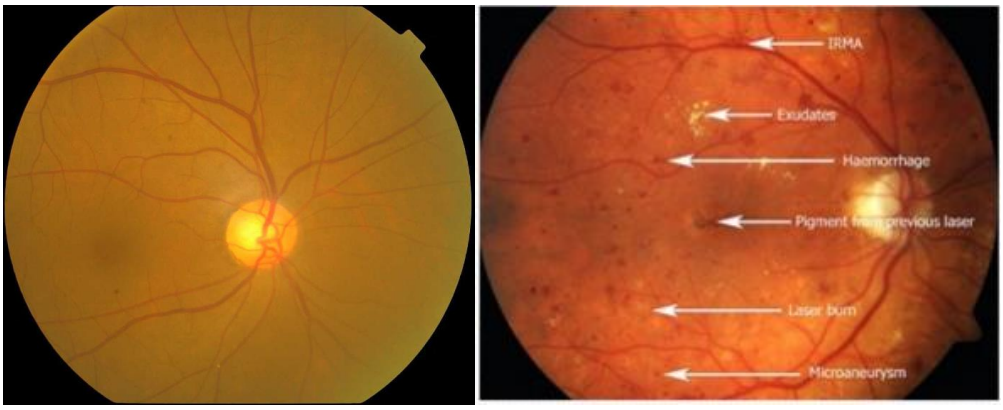

Figure 2-3 Fundus image of: (a) a Healthy normal Retina (b) Diseased retina showing a combination of DR symptoms [8]

2.3.1. Non-proliferative Diabetic Retinopathy (NPDR)

NPDR is the first stage of Diabetic Retinopathy and is categorized from mild to very severe characterized by specific symptoms of each severity level.

(1) Mild NPDR

When viewed using Fundus images of the eye Mild NPDR is marked by at least one **Micro aneurysm** in the retina (Figure 2-4 (a)) High sugar levels for prolonged durations weaken the retinal vessel walls leading to dilation of vessels followed by tiny out pouching of the capillary walls. These outpouchings are called Microaneurysms (MA) and appear as small sharp red dots in the temporal arcs of the fundus. MAs are more clearly seen as white dots in Fundus fluorescein angiography (FFA) where a fluorescein dye initially injected in an arm vessel is used to carefully examine the tiny retinal vessels as shown in figure 2-4 (b) below.

As the capillary network is effected, the body prepares to prevent **ischemia** (absence of oxygen), vessels dilate to ensure blood supply to the affected area. In diabetic cases, more of venous dilation is seen. In addition to that the veins also become **tortuous** (an increase in the twists and turns) to cover more surface area. Arteriolar dilation and twisting is more of an indication of hypertension. Figure 2-5 shows the difference between a normal vascular network and that having tortuous vessels.

Tortuosity of vessels is an inevitable early symptom to detect retinopathies.

(a) (b)

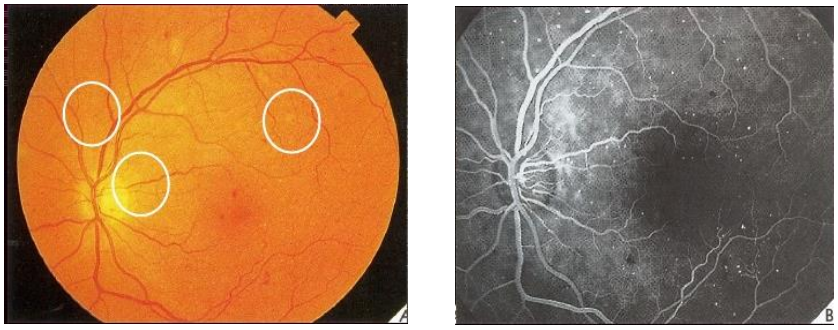

Figure 2-4 (a) Microaneurysm (MA) (b) FFA image of MA [8]

(a) (b)

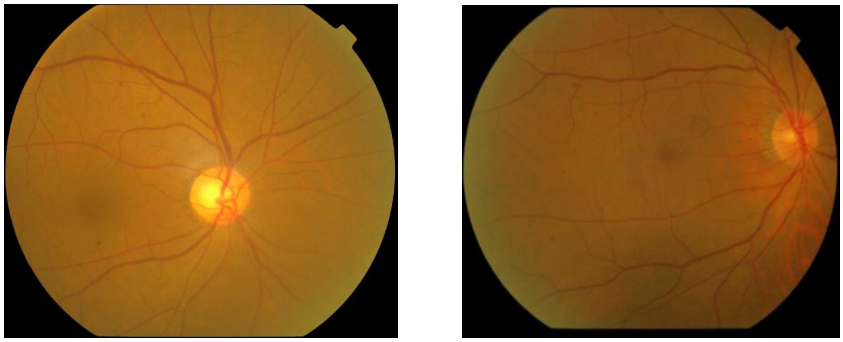

Figure 2-5 Fundus image showing (a) Normal vascular network (b) Venous tortuosity

(2) Moderate NPDR

In time, more vessels are effected by DR and the MAs increase in number. Eventually the MAs rupture to form **dot-blot like hemorrhages** (figure 2-6) in the Internal Limiting Membrane (ILM) of the retina [4]. **Splinter or flame hemorrhages** (figure 2-7) also appear in the temporal region. Both of these are small hemorrhages and are named in accordance to their appearance. The latter are also a characteristic finding in hypertensive patients.

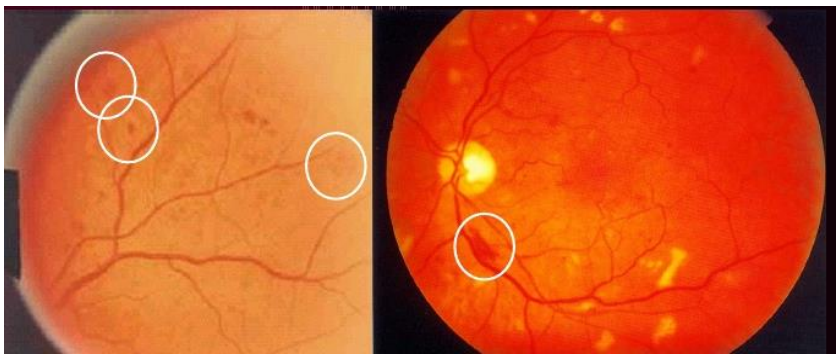

Figure 2-6 Dot and Blot intra-retinal hemorrhages, Notice the dot like appearance in left figure and a blot in the right one [8]

(a) (b)

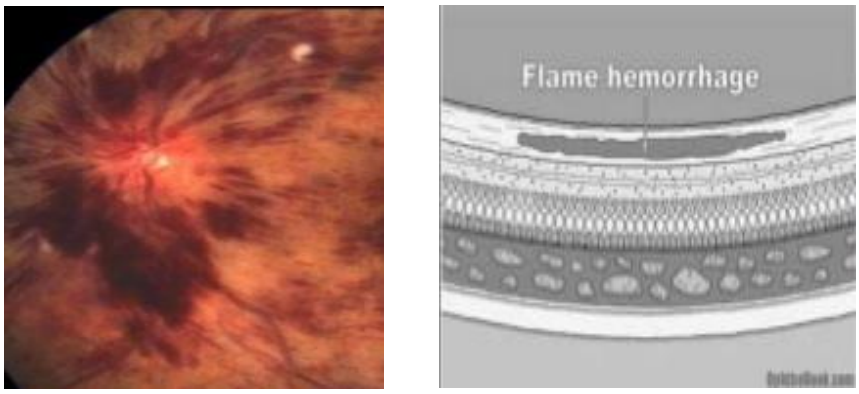

Figure 2-7(a) Flame hemorrhage (b) a representation of how a flame appears in the retinal layers [8]

The weakened vessels also begin to leak and the fluid begins to collect in the macula (an area in the center of the retina Figure 2-2), a condition known as **Macular edema,** shown in figure 2-8 a). The buildup of fluid causes the macula to swell and thicken, severely hampering vision or even causing blindness.

Over time as the fluid reduces it leaves behind lipid sediments, which appear as **hard white exudates** in the fundus. They are commonly found in a circular arrangement around the leaking MAs that lead to the exudates [9].

Figure 2-8 Lipid exudates as a result of macular edema [9]

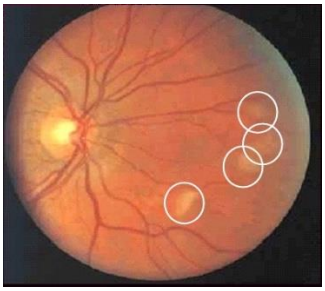

Figure 2-9 Cotton wool lesions in posterior eye [9]

As the disease prolongs, the nerve fiber in the posterior eye (area behind the lens) is affected too. Where the nerve is of considerable thickness, areas of dead tissue (infarcts) begin to form in the nerve fiber layer. This results in soft exudates that appear as **white cotton wool** lesions in a fundus image as shown in figure 2-9 above.

Figure 2-10 significantly tortuous blood vessel

Venous tortuosity increases too and appears more as kinks in the vessels (figure 2-10).

(3) Severe NPDR

In severe NPDR the pathological progress includes more pronounced symptoms from moderate NPDR in addition to the following:

Venous Beading (and/or looping): refers to the dilation and thinning of the venous caliber due to weakening vessel walls and ischemia in the affected area. This could also be accompanied by venous looping or ‘’omegas’ a name indicating the shape of the symptom. Figure 2-11 gives a clear representation of what it looks like.

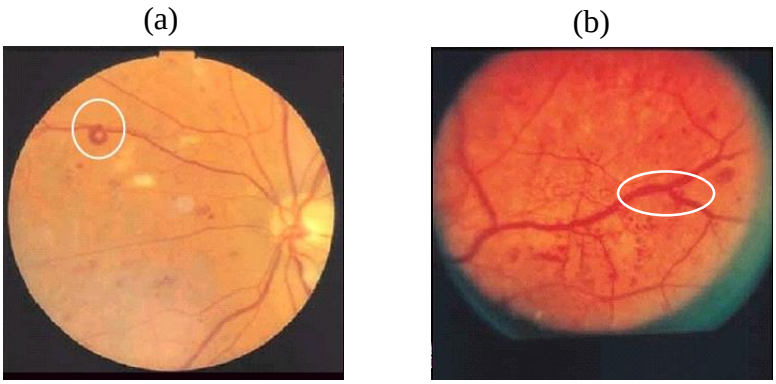

Figure 2-11: (a) Venous looping (omegas) (b) Venous beading notice the dilation and thinning [9]

IntraRetinal MicroVascular Abnormalities (IRMA)

As more and more vessels weaken and rupture, ischemia in multiple areas worsens. Stimulated by hypoxia (lack of oxygen), rearrangement of old vessels occurs or new vessels are formed. These typically form from one arteriole to a venule to renew blood supply to the region (Fig 2-12). These vessels are the most prominent feature of IRMA. The new vessels formed are very tortuous and irregular and are confined to internal retinal layers. Moreover, these vessels appear in a broad arrangement and appear to be thicker (or more dilated) than those in Neovascularization (discussed below). Irma is also more clearly distinguishable from new flat retinal vessels in a Fundus Fluorescein Angiography (FFA) because the new vessels leak profusely whereas IRMA shows minimal leakage in the later stages of angiography [10]

(a)

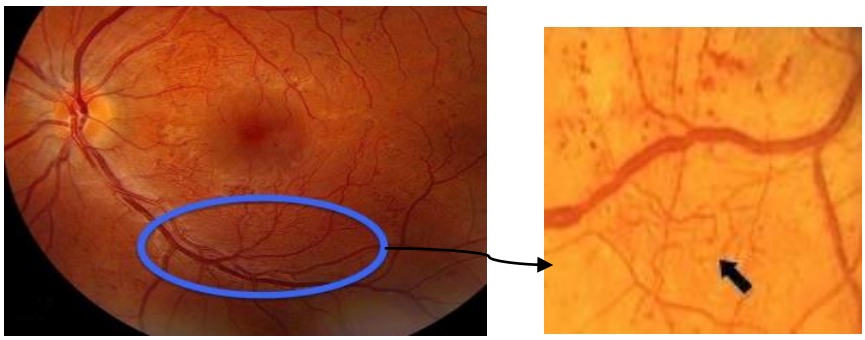

(b)

Figure 2-12(a)Magnified Image showing IRMA (b) A very clear Shunt vessel developed due to IRMA [11]

Venous beading and IRMA are very prominent features of an onset of PDR. Most of the patients that have reached this stage will reach PDR in a very short time. For this reason it is crucial to detect and treat DR as soon as possible.

2.3.2. Proliferative Diabetic Retinopathy (PDR)

PDR is the most severe level of DR in that new vessels start forming in the Internal limiting membrane and over the retinal vessels severly obstructing image and causing blindness.

The new vessels either form near or on the optic disk referred to as Neovascularisation of the disc (NVD) or elsewhere on the retina known as neovascularisation Elsewhere (NVE) as in figure 2-13 and 2-14 respectively. These vessels often grow randomly and are weak and leaky. If the leaked fluid causes enough traction, it can lead to seperation of retinal layer.

Figure 2-13 NVD

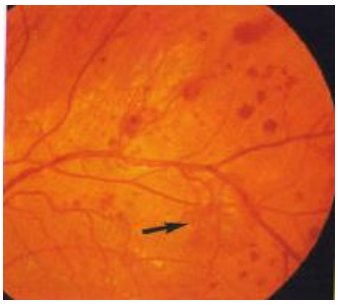

Figure 2-14 NVE

Retinal fundus images are colored images obtained through specially designed cameras through dilated pupil of the patient. Analysis of these images is being used to detect retinal abnormalities to provide insight into onset or severity of retinopathies specially hypertensive or diabetic retinopathy.

2.4. Tortuosity

In this thesis, we develop a technique to identify IRMA in the given fundus images through detection of vessel tortuosity. Tortuosity refers to how twisted a curve is or how many turns it has. The simplest formula used to calculate it is the arc-chord ratio:

$$T=L/C \tag{2.1}$$

Where L= arc length of the curve, C = the distance between the two ends of the curve.

In context to the eye, tortuosity needs to be explained more explicitly. Since a normal vascular pattern may have a few curves present as part of the normal anatomy of an individual, tortuosity is defined as the kinked appearance of a vessel, which means that instead of the usual smooth curves the vessel starts exhibiting a sudden-frequent turn pattern.

Detection of change in the tortuosity of the retinal vascular network can help to differentiate between a normal and an abnormal pattern. The presence of vascular tortuosity in the eye or an increase in it is usually among the first anatomical modifications to occur in retinopathies.

It is interesting to note, that hypertensive retinopathy usually causes arteriolar tortuosity whereas Diabetic retinopathy mostly affects the venular appearance.

As discussed in the section above, along with other characteristic symptoms of each stage, the retinal vascular pattern shows varying tortuosity in different stages of DR. The forming of hemorrhages and micro aneurysms causes weakening of the retinal vascular walls. This affects the blood supply and hence the amount of oxygen reaching that area. As a defense mechanism,

the body prepares to prevent ischemia (or decrease of oxygen) in the locality. The vessels dilate and become more tortuous to cover up a larger surface of the retina and hence ensure blood supply. Figure 2-15 and 2-16 show a normal vascular network and one with tortuosity, respectively.

Figure 2-15 Normal Vascular network

Figure 2-16 Venous tortuosity

If not controlled in time, DR may worsen and cause further changes in the vascular network. As DR progresses from mild non-proliferative to its severe level, more vessels are weakened and are unable to maintain the required blood supply. To prevent a total cut off of oxygen to the tissue, old vessels rearrange themselves or random new vessels are formed. These new vessels usually appear as small kinked vessel that connects an artery to a vein. This is referred to as IntraRetinal MicroVascular abnormality and needs instant attention. At this stage if not treated or controlled, DR may lead to permanent blindness in a very short duration.

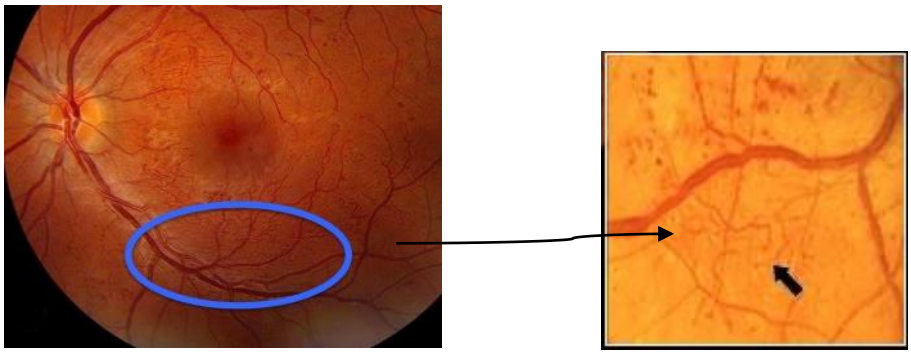

Figure 2-17 Magnified image showing IRMA

The automated detection of tortuosity and IRMA by analysing the vascular structure can act as an important non-invasive technique for early detection of DR and various diseases.

3. Literature Review

Tortuosity, the number of turns or twists, has been long used in different fields as an entity to define a certain shape or as a supplementary feature to give additional insight to the characteristics of an object. In biomedical engineering, it is used as a significant anatomical detail that gives useful information regarding any harmful changes occurring in the body. For instance, tortuosity of the bone can help determine its fragility [12] and unusual vascular tortuosity for example of the intracerebral region [13] is one of the early indicators of a health issue. In this thesis we focus on eye vessels, that is the retinal vascular tortuosity.

A change in the shape of these vessels is one of the first symptoms of the onset of different retinopathies, example hypertensive retinopathy, Diabetic retinopathy, retinopathy of prematurity (RoP) [14] etc. This chapter gives the state of the art techniques being used to determine vascular tortuosity of the retina and explores how much work has already been done in this context. The techniques used to calculate tortuosity are generally divided into three main categories:

1) Distance approach: which primarily use the ratio of the actual distance between two ends of a vessel segment to the shortest path between them

2) Curvature approach: relies mainly on determining the deviation of a vessel from a straight line through different mathematical formulae. The curvature may be calculated at each point of a vessel segment or over a small portion.

3) Hybrid techniques: that incorporates a mixture of the two previous methods and may use additional features such as thickness, width, diameter etcetera of the blood vessels to quantify tortuosity.

[15] Also gives detailed overview of the methods used in each approach and their respective mathematical details.

Most of these techniques, usually require preprocessing steps which primarily involve the following steps (and will be explained in detail with the methodology)

1) Background Noise Removal
2) RGB to grayscale conversion
3) Vessel segmentation (and skelotonisation)
4) Extracting long unbranched arcs
5) Quantifying tortuosity.

3.1. Distance based techniques:

Lotmar et al [16]proposed the basic Arc to Length ratio which uses the ratio of actual length of the vessel to its chord length as shown in figure 3-1, in order to calculate tortuosity of one vessel or a vessel segment.

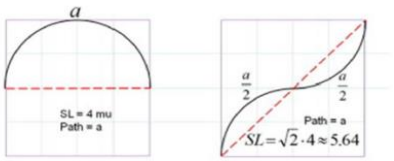

Figure 3-1 Arc to length ratio of two different curves

For a global value of tortuosity, all individual values are summed up and divided by the number of vessels to get an average value,

$$\textbf{Average tortuosity} = \frac{\sum_{k=1}^{n} T(k)}{n} \tag{3.1}$$

Where T (k) = tortuosity of the kth vessel segment and N= total number of vessels.

Though this formula is still used in quantifying tortuosity, it is seldom used on its own because it cannot distinguish a large curved section from a section with more, but slight curves as can be seen in figure 3-1.

3.2. Curvature based Techniques

The curvature of a planar curve defined as γ (t) = (x (t), y (t)) is parametrically given as

$$k = \frac{x'y'' - y'x''}{\left(x'^2 - y'^2\right)^{3/2}} \tag{3.2}$$

Hamid Pourreza [17]proposed a basic and effective algorithm for grading tortuosity in the fundus images. This algorithm uses a modification of the planar curve equation given above. It applies a circular mask, such that the center of the mask is placed on every point of the vascular skeleton. Circles having 3 or 4 intersections denote bifurcations or loops and are eliminated. Tortuosity for each curve is then measured as the ratio of area of the larger segment to the area of smaller segment (since the curve divides the circle into two uneven areas) as shown in figure 3-2. Tortuosity, k2 is given by:

$$k_2 \approx \frac{A}{A_{tot}-A} \tag{3.3}$$

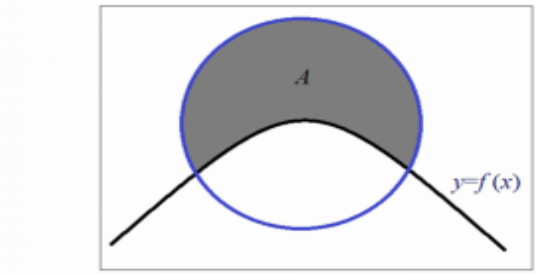

Figure 3-2 Curvature calculation using a circular mask

The k2 equation is a simplification of following equation (derived from the planar curve formula).

$$k_1 \approx \frac{3\pi}{b}\left(\frac{A}{A_{tot}}-\frac{1}{2}\right) \tag{3.4}$$

Where b= radius of the circle, A= gray area in figure 3-2, Atot = area of full circle

Global tortuosity of the image is an average of all the curvatures "k2" calculated for "m" number of points.

Their algorithm's performance was evaluated over Grisan's dataset and one from Khatam-Al-Anbia Hospital, Iran and achieved a Spearman correlation coefficient of over 85% and 95% respectively.

Farnoosh [18]proposed an alternative curvature based technique where a grey scale image is obtained from the RGB image and circles are placed along the curvatures of the vessels using circular Hough Transform. The image is divided in to equal sized windows, assumed to have uniform illumination. Concentric circles are placed on each boundary of one vessel (as shown in figure 3-3) using Tao Peng's algorithm (from Matlab File exchange). Then a weighted technique is used to eliminate concentric circles forming due to noise, branches or intersection of vessels.

Major Weightage is given to smaller concentric circles with closer radii, which actually depict a curve in the normal vessel flow. Closer radii are multiplied by 1 while larger circles with a greater radii difference are multiplied by 0.5.

Tortuosity is calculated using:

$$Tortuosity = 1/\mathrm{n}(\sum_{i=1}^{n}\left(\frac{w_i}{r_i}\right)) \tag{3.5}$$

Where n is number of detected curves, "ri" is radius associated with each curve and "wi" is product of normalized accumulator value with 1 or 0.5.

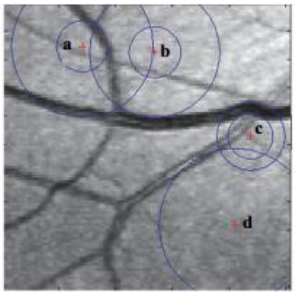

Figure 3-3 Result of Hough transform, only two concentric circles (with center 'c') with close radius, are positioned correctly on a curve

The algorithm was tested on database consisting of 40 images, mixture of DRIVE database and images from Khatam-Al-Anbia Hospital. The proposed algorithm achieved a classification rate of 92% along with less computation time compared to previous methods.

Another algorithm by Enrico [19] is based on the partitioning of each vessel in segments of constant sign curvature and on the combination between the number of such segments and their curvature values. The curve is decomposed into a set of consecutive segments of constant curvature sign and is based on two assumptions

i. the greater the number of sign changes in a vessel, the greater the tortuosity
ii. the greater the amplitude difference of a segment from the respective chord, the greater the tortuosity

The vessel tortuosity is then calculated from the following formula

$$T(s) = \frac{n-1}{Lc}\left(\sum_{i=1}^{n}\left(\frac{L_{csi}}{L_{xsi}}\right) - 1\right) \tag{3.6}$$

Where n is the number of curves detected, Lc is the segment length and Lx is the chord length of a segment. They also tested multiple tortuosity measures (from literature) on veins and arteries and prove that arc length over chord ratio is the most robust method to determine tortuosity

Masoud [20]proposed a curvature based methods which uses modification to the template disk method to calculate the curvature of different points on a sub vessel.

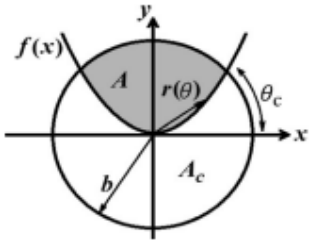

Figure 3-4 Curvature calculation with the template disk method

The planar curvature equation for y =f(x) shown in the figure 3-4 is given by:

$$k = \frac{y''}{(1 + y'^2)^{3/2}}$$

To determine the curvature, a template disk of radius b is positioned at every co-ordinate (x, y), then that point is superimposed on the origin. Then, using a series of assumptions on the Taylor series of f(x), assuming a small angle, and hence a smaller disk radius and integrating it into the curvature formula given above, the following simplified equation is obtained:

$$\kappa \approx \frac{3\Pi}{2b} - \frac{3A}{b^3} = \frac{2A_c}{b^3} - \frac{3\Pi}{2b} \tag{3.7}$$

Where Ac is the complement of A and b is the radius of the template disc. From this equation, a non-linear equation of the curve can be given as follows:

$$\kappa_{nl} \cong A_c \tag{3.8}$$

A. 1st Modification: tortuosity using the crossover point.

As mentioned earlier, the curvature can be estimated by the area between the curve and the disk. In this case, the total area is given by the gray area plus the green area. But the green area is negligible as can be seen in figure 3-5, hence the total area can be approximated by the gray area A'.

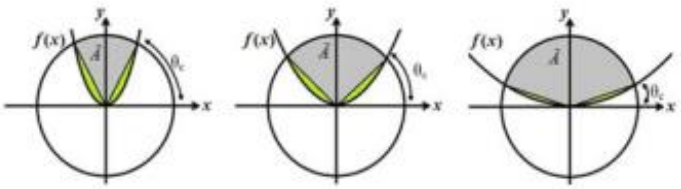

Figure 3-5 Approximating area A using crossover of curve and template disk

Through a series of mathematical calculations, detailed in [20] the curvature is defined as the squared reciprocal of A'.

$$\kappa_{cp} \cong \frac{1}{A^2} \tag{3.9}$$

B. 2nd Modification: Trignometrical Method

A direct relation is obtained between the cross over angle and curvature. Given by:

$$\kappa_{tr} \cong \frac{2 \sin \theta_c}{1-2 \sin {\theta_c}^2} \tag{3.10}$$

These three different formulae are used to calculate retinal vessel tortuosity at every point on the extracted sub vessels.

The global tortuosity is then calculated using:

$$\tau = \frac{1}{m} \sum_{i=1}^{m} \kappa_i \tag{3.11}$$

Where ki is the curvature on an ith point on the image.

From the results, it is shown that these measure give good results when comparing tortuosity on a vessel level.

3.3. Hybrid techniques

As mentioned above, Hybrid techniques involve a combination of parameters which help determine the tortuosity using a combination of the aforementioned techniques.

Arunaya et al [21] used Quadratic Polynomial Decomposition (QPD); in which the ideal vessel is modelled as a quadratic polynomial at a larger scale while the deviations are modelled as

quadratic polynomials at smaller scales. A given vessel centre-line is decomposed as a sum of quadratic polynomials of decreasing scale. This Quadratic Polynomial Decomposition is used as a framework for defining a quantitative measure of tortuosity.

Vishnu [22] proposed a tortuosity calculating measure that is based on angular calculations. As a pre-processing step, Moore's algorithm is used to traverse the vascular skeleton to remove all branches; hence the given algorithm works only on the major vessels assuming that there are no branches or loops.

For a given number of N points on the vessel, three vectors are drawn for each point Pi (as shown in the figure 3-6). The Vectors- vi- are defined as follows:

$$\bar{v}_1 = P_i - P_{i-1} \tag{3.12}$$
$$\bar{v}_2 = P_{i+1} - P_i$$
$$\bar{v}_3 = P_{i+2} - P_{i+1}$$

Then angular bisectors are drawn to get an estimate of the angle at point Pi. The angles a1 and a2 are actually perpendicular to the ones shown in the diagram and hence give the angle at point Pi as it would be from a horizontal axis.

$$\tilde{\alpha}_1 = \frac{\bar{v}_1}{|\bar{v}_1|} + \frac{\bar{v}_2}{|\bar{v}_2|} \tag{3.13}$$
$$\tilde{\alpha}_2 = \frac{\bar{v}_2}{|\bar{v}_2|} + \frac{\bar{v}_3}{|\bar{v}_3|}$$

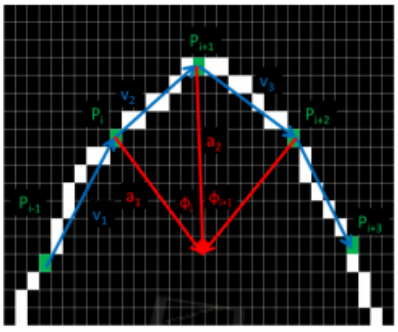

Figure 3-6 Angle measured between the angular bisector near the end of a curve.

The angle Øi is given by

$$\Phi_i = cos^{-1}(\tilde{\alpha}_1 . \tilde{\alpha}_2 / |\tilde{\alpha}_1||\tilde{\alpha}_2|) \tag{3.14}$$

This angle determines the tortuosity of the curve. As can be seen from the diagram, the larger the curve, the greater the angular value. For smaller curves or straight lines, the angle between the bisector decreases as the lines tend towards becoming parallel.

Tortuosity of a vessel is given by

$$Tortuosity = (\Sigma \Phi_i) / ((\Sigma |P_i - P_{i-1}|)) \quad (3.15)$$

It was tested on a set of 30 curves and gave a good 0.8901 spearman Correlation Coefficient.

Nidhal et al [23] algorithm uses the formula of arc length over chord length ratio to calculate tortuosity but uses image labelling algorithm to detect the blood vessel segment. Each segment is given a label using the image labeling algorithm and the results stored in a union find table. The union find table is used to resolve equivalence class issues and maintain non overlapping finite sets. The following mask in figure 3-7 is used on each blood vessel segment and nine possible orientations are obtained. Mask movement is based on the result of the mask and the overlapping image, with the mask center always being on the current pixel.

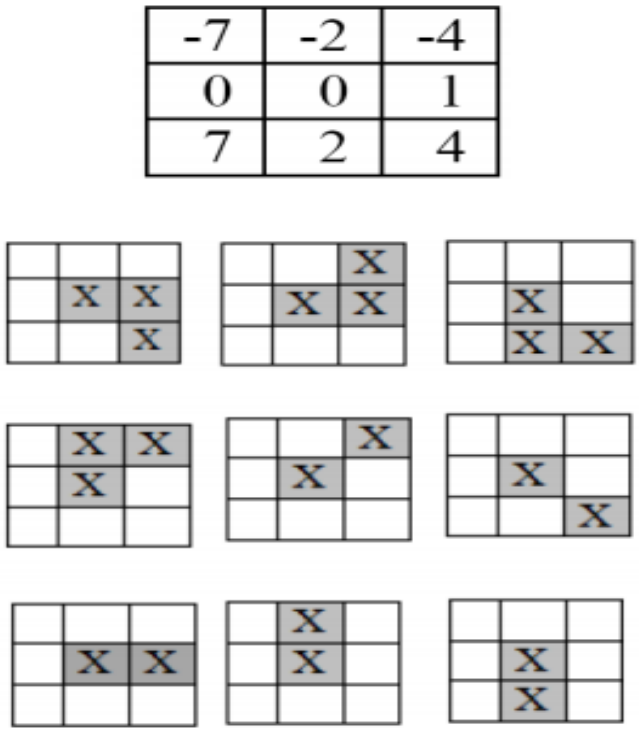

Figure 3-7 Filter mask and its movement

As the mask moves from left to right, the segment length keeps adding a 1 or √2 depending on the result obtained from overlapping the mask and the image. Hence the arc length of a segment

of the blood vessel is obtained. The chord length is calculated using Euclidean distance on the end points of the segment. This technique was tested on hand drawn lines and curves and gave accurate results.

Ernesto [24] uses the Slope chain code (SCC) to compute the tortuosity of the vessel. SCC of a curve is obtained by placing constant length (l) straight lined segments on the curve such that the endpoints of each line segment are touching the curve. Hence, the smaller the line segment the better the curve representation and greater the computational requirement.

The lines are then represented in terms of slope change ranging from -1 to 1, in reference to the previous line. This gives a chain of codes that represent the curve. This is done by superimposing circles of radii equal to the previous line segment that traverse the curve as shown in figure 3-8 below.

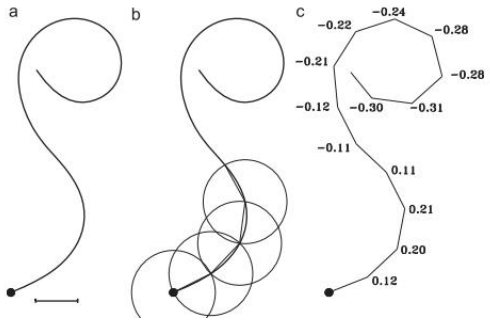

Figure 3-8 superimposing circles of equal radii to traverse the curve

The tortuosity of each vessel is the absolute sum of all the slope values and normalized Tortuosity is given by total tortuosity divided by the number of slopes. This technique was presented as a general measure of tortuosity but was tested on retinal vascular structure.

Another chain code method by Danu Onakew [25] uses a method named as improved code chain to evaluate the curvature of a vessel. The algorithm uses laplacian of Gaussian followed by Otsu thresholding to extract the vessel center line. Once that is done, vessel segmentation is obtained using “four connectivity in eight neighborhood” method to determine the end points and branch points of the vascular tree. Then for each pixel on the partitioned vessel, the curvature κ is calculated using the following three staged equation

$$\kappa\,(p_i\,,\mathrm{k}\,) = 1/k \sum_{j=1}^{k} \begin{matrix} \{\min\left(f'_{i+j}\,,8-\,f'_{i+j}\,\right), \\ \min\left(f_{i+j}^{\prime(+1)}\,,8-\,f_{i+j}^{\prime(+1)}\right), \\ \min\left(f_{i+j}^{\prime(-1)}\,,8-\,f_{i+j}^{\prime(-1)}\right)\} \end{matrix} \tag{3.16}$$

where $\left(f'_{i+j} = |f_{i+j} - f_{i-j+1}|\,\right), \left(f_{i+j}^{\prime(+1)} = |f_{i+j+1} - f_{i-j+1}|\,\right), \left(f_{i+j}^{\prime(-1)} = |f_{i+j} - f_{i-j}|\,\right)$

Are the chain code of the jth leading and following point with respect to point of interest pi respectively. K is the number of points used for curvature calculation and is equal to 8 in this paper. Since any vessel can have a number of twists, only the points with high curvatures are selected using a threshold value. These numbers of inflection points, n, are then used in the following formula to calculate vessel tortuosity:

$$\tau = \frac{n_{ic}-1}{n_{ic}} \frac{1}{L} \sum_{i=1}^{n} \kappa\,(p_i\,,\mathrm{k}\,) \tag{3.17}$$

Where n_{ic} is the number of inflection points and L is the arc length of the vessel.

Global tortuosity is calculated as a sum of the tortuosity of the sub vessels using only tortuosity values higher than a certain limit, in this case 0.3 for arc lengths greater than 20 units. Threshold is calculated in the training phase, using

1. Mean of maximum tortuosity values in normal images
2. Mean of minimum tortuosity value in diseased images

They used an unsupervised learning mechanism on a dataset of eighteen images, 10 of which were used for training and the remaining 8 for testing.

Another recent paper [26] presents the effect of DR on retinal vasculature using the modified template disk method proposed by Masoud [20]. It calculates the tortuosity of an image and classifies it as tortuous or non- tortuous against a threshold calculated by the method described in Danu Onkaew's paper [25]. The same images are also categorized in to DR or no-DR by determining other DR symptoms such as microaneurysms, cotton wool spots and exudates.

The findings were then correlated and it was found that there is a very vague relationship of DR with tortuosity of the retinal vessels. Hence, more research is required to further establish the effects of DR on vessel tortuosity.

4. Methodology

To review the problem, Diabetes is one of the leading illnesses causing multiple complications in a human body. Diabetic Retinopathy (DR) is one such implication of Diabetes that affects different regions of the eye including the retinal vessels. Initially, the vessels become tortuous but the symptoms accelerate quickly and may cause irreversible damage leading to blindness. DR is a common problem among the low income, working class population. To preserve the health of these individuals, it is vital to provide a platform that makes eye health analysis accessible. This research tries to resolve the problem by providing an automatic platform to indicate the presence of an abnormality, if any, at an early stage to ensure a timely course of action. We do so by detecting the presence of tortuous vessels in a fundus image.

This research presents a method for segmentation and classification of retinal vessels from Ocular Fundus images to determine Intraretinal MicroVascular Abnormalities. We first discuss the segmentation technique followed by the classification procedure.

In general the implemented algorithm can be broken down into the following steps:

1) Background Noise Removal
2) RGB to greyscale conversion
3) Vessel segmentation (and skelotonisation)
4) Extracting long unbranched arcs
5) Calculations to determine feature set.
6) Classification of normal and tortuous vessels

Segmentation

Classification

Figure 4-1 depicts the flow of the process.

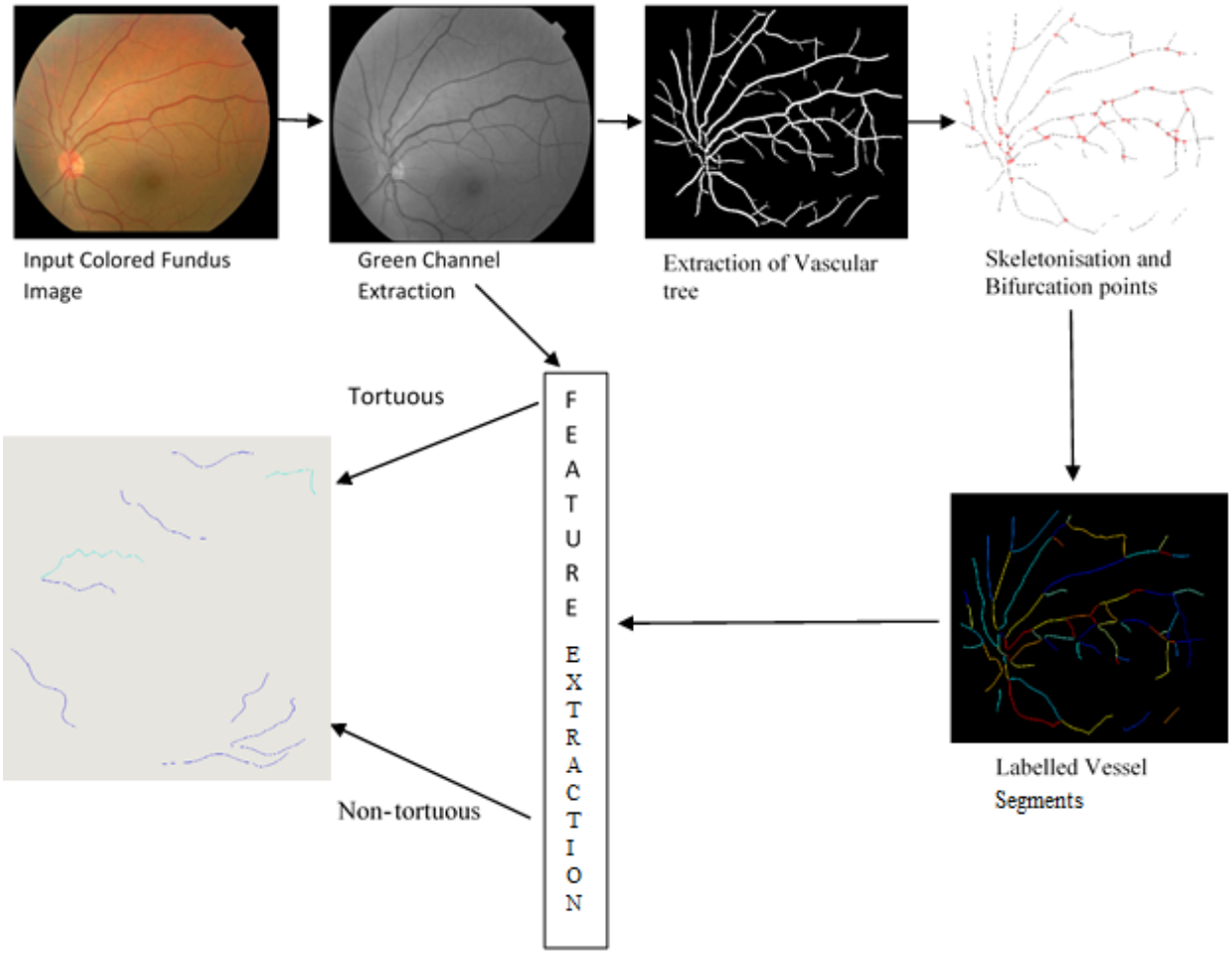

Figure 4-1 Flow Chart of Methodology (skelotonised image is shown in white background for clarity)

4.1. Segmentation

In digital image processing, segmentation is a process to partition the image to extract more meaningful information from it. In dip jargon, that is termed as the Region of Interest(ROI). Fundus images are pictures of the internal eye taken through a special camera. In our fundus images, the region of interest is the vascular network tree. After acquiring the retinal vessels and a few post processing steps, the image is ready for feature extraction, these extracts are then used for classification.

4.1.1. Background Noise Removal

An ideal fundus image has optimum illumination and nearly zero noise which then gives a clear picture of the internal ocular structures. Practically, this is not achievable. So our first objective is to separate the foreground and background pixels followed by removal of any background noise from our input- a colored fundus image. For our case, noise is any extra area or presence other than the retinal picture. To eliminate it, we create a mask that helps us select the retina only. This requires a series of steps as follows: we first extract the green channel from our image to get a rough boundary of where our Region of Interest (ROI) exists, and then pass it through an 11x11 median filter. Median Filters (MF) are used to smooth the picture and detect edges. A window (11x11 for our technique) is centered on each pixel of the image, where the center pixel is replaced by the median value of the neighborhood. Figure 4-2 displays the steps involved.

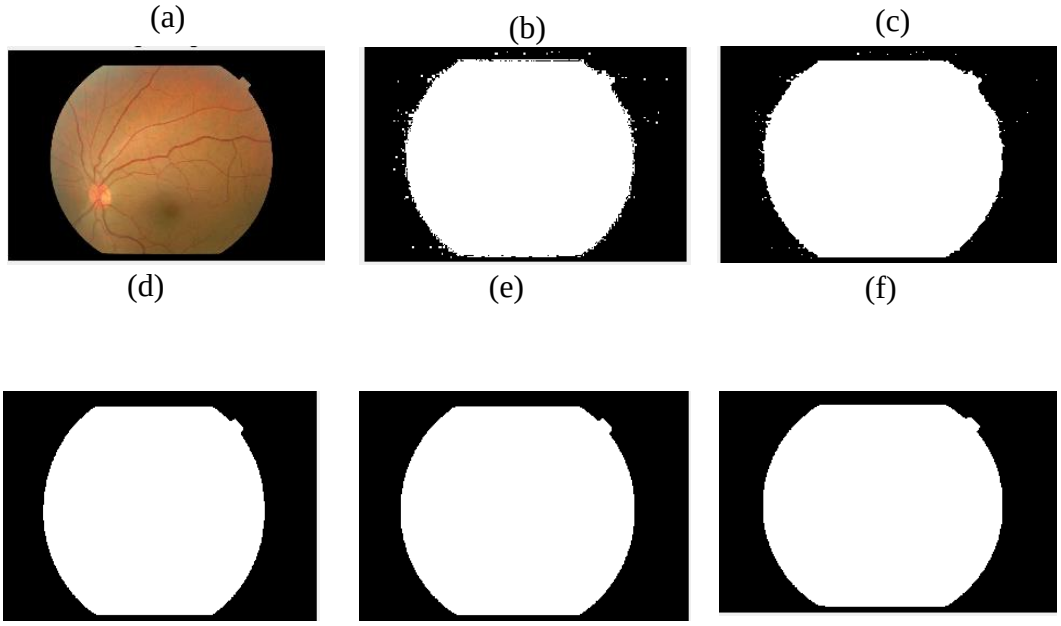

Figure 4-2 Steps to remove any background noise (a) Colored Input Image b) Threhsolding (c)Image after applying the median filter (d) removing small spurs and filling in holes (if any) (e)Minor Erosion with a disk of radius 5 (f) resultant mask

The mask then goes through two morphological operations, as discussed further.

Morphological Operation: Opening and Erosion

Morphological Operations help to remove imperfections in an image primarily using a combination of two processes: Erosion and Dilation

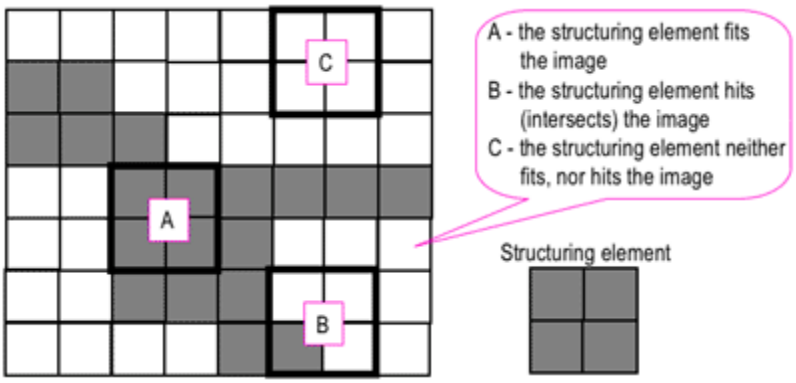

Figure 4-3 Probing of an image using a square structuring element [27]

The result of interaction of the structuring element with the input image is dependent on different criterion as shown in figure 4-3:

A- Fit: When placed on the center pixel, the structuring element (SE) covers all 1s (or on /true pixels). The SE is said to fit the image.

B- Hit: If the area under the SE covers at least one but not all true pixels, that is the center pixel or some of the neighborhood pixels are 0, this is termed as a hit

C- Neither: the SE covers all false pixels, in which case the whole SE is multiplied by 0 giving a 0 result.

Erosion

$$B = (A \ominus SE) \tag{4.1}$$

Where A is the input image and SE is the structuring element.

B=1 if SE fits after its placement on the center pixel it is applied to, in A, else B=0. Generally, erosion removes a layer of pixel from the inner and outer boundary of the object it is applied to and hence enlarges any gaps or holes, eliminating detail.

Dilation

$$B = A \oplus SE \tag{4.2}$$

Where B=1 even if SE hits the image A. hence, it adds a layer of pixel to the inner and outer boundary of the image it is applied on [28].

Opening

Opening is a morphological operation defined as erosion followed by dilation. It uses the same structuring element for both operations. Consider A as an input image and SE as a structuring element then opening can be represented as:

$$A \circ SE = (A \ominus SE) \oplus SE \tag{4.3}$$

Opening is used to separate objects since it thins boundaries and then reconstructs some of it.

Closing

Closing is the opposite of opening: it is dilation followed by erosion and uses the same structuring element for both the operations.

$$A \circ SE = (A \oplus SE) \ominus SE \tag{4.4}$$

Closing is usually done to fill gaps and then remove the extra boundary that forms around the object through erosion.

Choice of Structuring Element

The choice of SE depends on the shape of the object, which will undergo a morphological operation and the required results. For example it is better to choose a circular shaped structuring element for rounded objects to preserve the characteristic properties of the shape. Using a square, might cause the edges to straighten up.

For the circular mask here, firstly a morphological area based opening was applied in that it removed any objects smaller than a certain area, removing small spurs, leaving us with one whole intact circle. This was followed by erosion using a disk of radius 5 as the structuring element to ensure an optimum size for the mask.

4.1.2. Vessel Segmentation

Vessel Segmentation comprises the most fundamental part of the segmentation process. The background mask from the previous step is used in combination with Fourier transform and Gabor wavelet, in that order, to extract our primary region of interest (ROI) - the retinal vascular network. We apply the segmentation and enhancement algorithm proposed by M Usman Akram in [29].

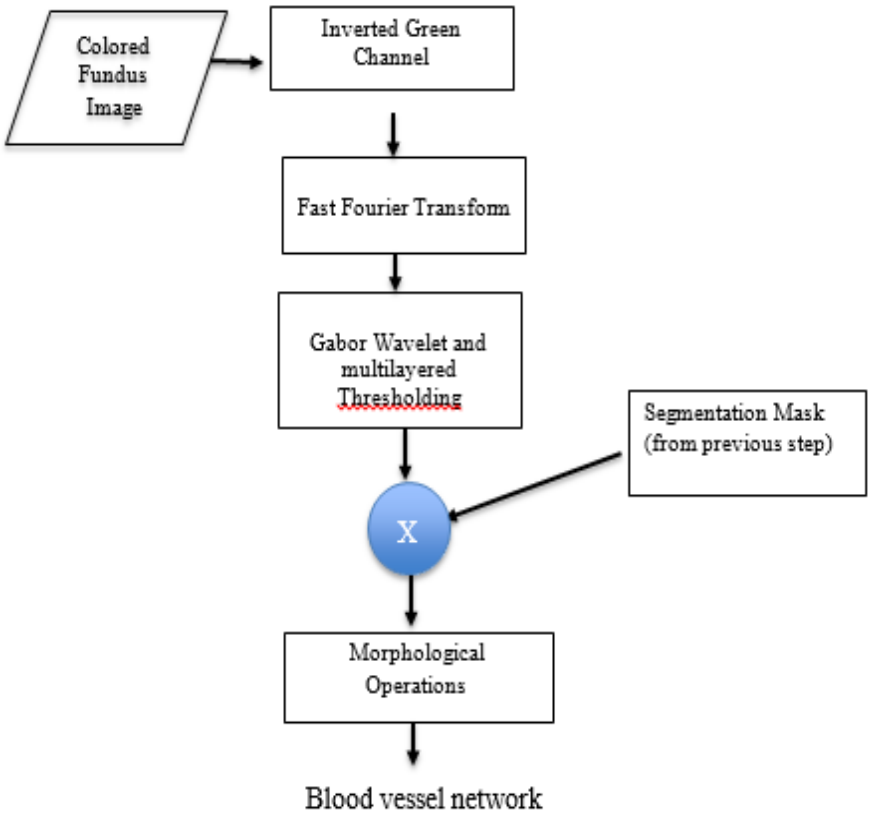

Figure 4-4 Flow chart of Vessel network Extraction

A Colored Fundus image is made up of three frequency channels, namely: Red-Green-Blue (RGB). Each band contains specific frequency information of the image. Usually, to reduce computational complexity, one channel is extracted for further processing. In our case, the Green channel contained most of the required details and hence was a good choice to move on with as shown in Figure 4-5. Complement of the green channel was used for better clarity.

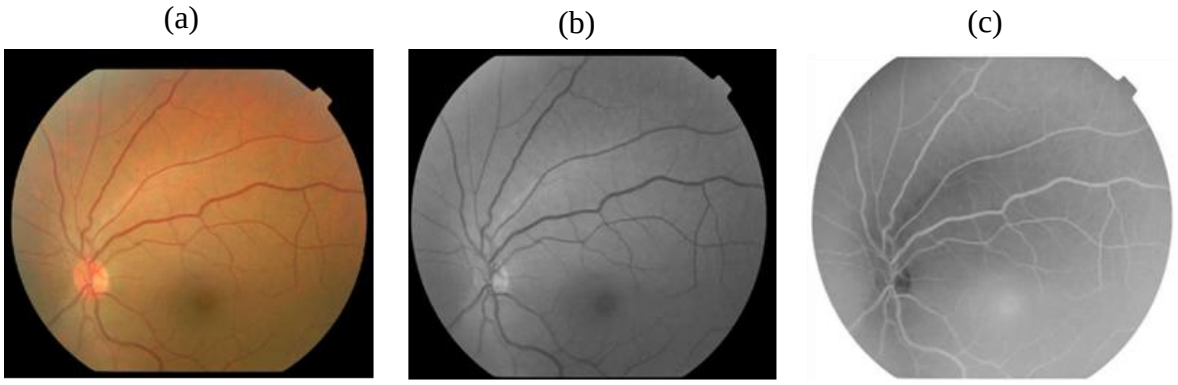

Figure 4-5 (a) RGB Fundus Image (b) Green Channel (c) Inverted green channel

The next step is to take the Fourier Transform of the image to be used by the Gabor wavelet. We take a brief overview of both the processes before stating how they are used in this algorithm.

FAST FOURIER TRANSFORM (FFT)

Commonly, signals that we see around us are represented in time domain- that is, how the signal looks over a certain time period but this does not give us the complete information of its components. This is mostly true for complex or multidimensional signals for instance an image which essentially is a 2-D signal.

Fourier Transform (FT) gives a frequency domain representation of these entities. It gives the sine and cosine components that the signal is composed of. Since this requires intense mathematical computation, usually a Fast Fourier algorithm is used to calculate FT which reduces the complexity of calculation. For images, this means taking discrete samples over the two dimensions because processing in continuous domain is nearly impossible, hence, it is called the Discrete Fourier Transform (DFT). For an image of size M x N, DFT is mathematically defined as

$$F(k,l) = \sum_{i=0}^{M-1} \sum_{j=0}^{N} {}^{-1} \left(f(i,j) e^{-i2\pi \left(\frac{ki}{M} + \frac{lj}{N} \right)} \right) \tag{4.5}$$

where *f(i,j)* is the image in the spatial domain and the exponential term is the basis function corresponding to each point *F(k,l)* in the Fourier space[2].

Similarly, the inverse of FFT brings the image back in to the spatial domain given by:

$$f(i,j) = \frac{1}{MxN} \sum_{i=0}^{M-1} \sum_{j=0}^{N-1} (F(k,l) e^{-i2\pi (\frac{ki}{M} + \frac{lj}{N})}) \tag{4.6}$$

The three transformations are shown in figure 4.6 below:

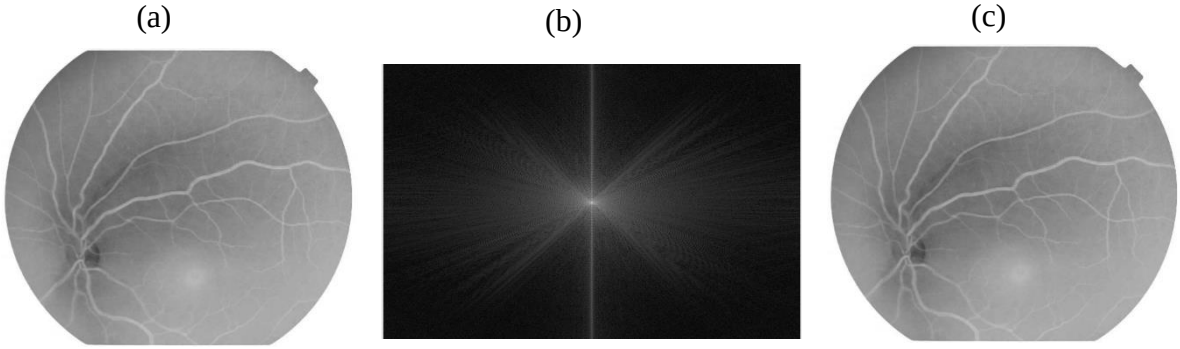

Figure 4-6 : (a) Original Image (b) Centered Frequency response (c) Inverse FFT

2-D Gabor Wavelet

A wavelet is a wave like pattern designed with user given specifications to extract particular information from an image. The image is cross correlated with the wavelet at different scales to know its components. One of the wavelet is called a Gabor wavelet, named after the scientist who discovered it. Figure 4.7 shows a typical Gabor wavelet.

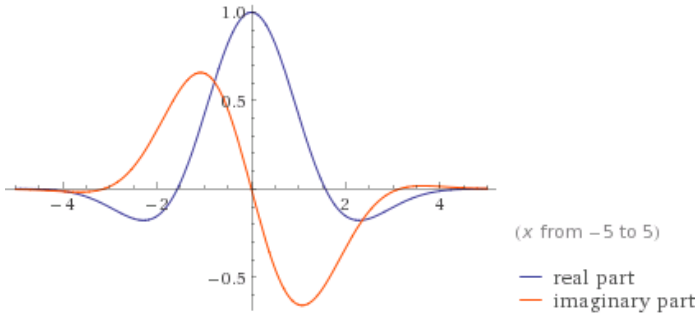

Figure 4-7 Gabor wavelet with a=2, x_0=0 and k_0 =1 [30]

Among other features, Gabor wavelets have a good accuracy in detecting varying shapes, sizes and edges and are said to have a response closest to human visualization [31] - both being useful attributes to detect the vessels. They can also be tuned for specific frequencies and orientations which is useful for both thick and thin vessels [32]. The 2_D Gabor wavelet is given by the equation [29]:

$$\varphi_c(x) = \ e^{jk_0x}e^{\left(-\frac{1}{2}|Ax|^2\right)} \tag{4.7}$$

Where k0 is a vector that defines the frequency of the complex exponential and A is a diagonal matrix that defines the scale and orientation of the wavelet.

The FFT of the green channel image along with other parameters defining the wavelet were used to iterativley calculate the maximum response wavelet. Fig 4-6 a shows the different orientations of Gabor wavelet, In (a) Notice the response being shown in the four corners.Centering the FFT makes it visually clearer as in (b). Each orientation of the wavelet is correlated with the image to determine the maximum response wavelet, which is then used for the final extraction stage. Figure 4-7(c) shows the correlation in frequency domain and (d) shows the area of the image that gives the best correlation result.

(a)

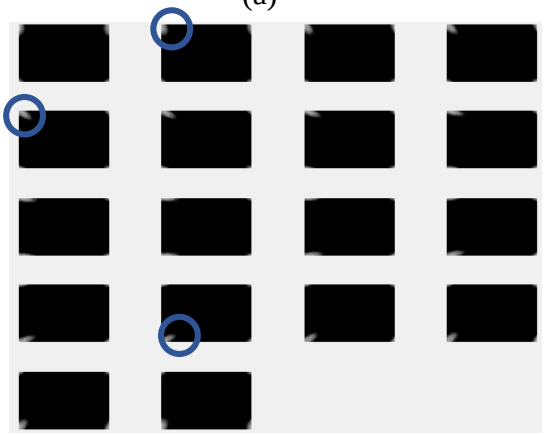

(b)

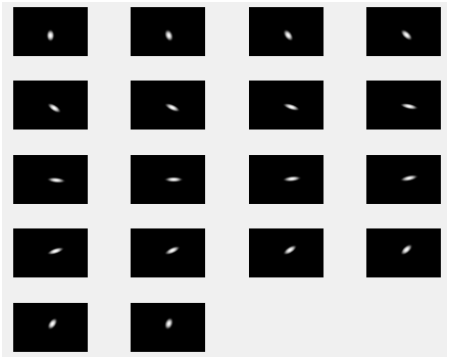

(c)

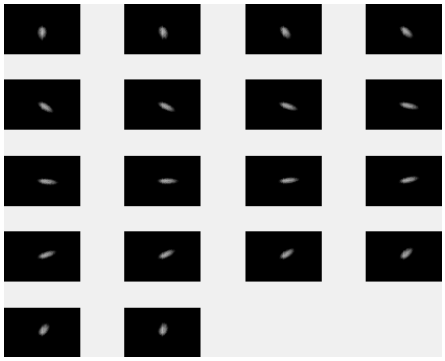

Figure 4-8 wavelet orientations and responses (a) FFT Gabor wavelet Orientation (b)Centered FFT response (c) FFT result of correlation with the image (d) results in the spatial domain

(d)

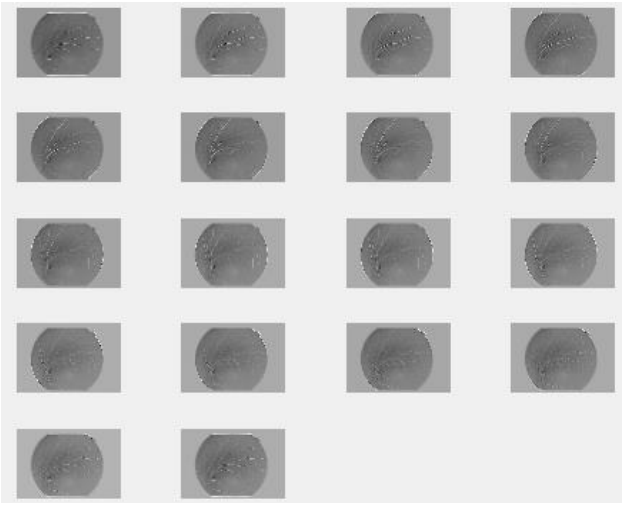

The resultant wavelet of the process is then multiplied with the image and the background mask to extract information in all the specific directions.

Once the vessel tree is extracted, a multilayered adaptive process is used to determine the best threshold to make the vessels clearer. [32]gives a detailed explanation of the process. Figure 4.9 shows a seperated vessel tree after thresholding.

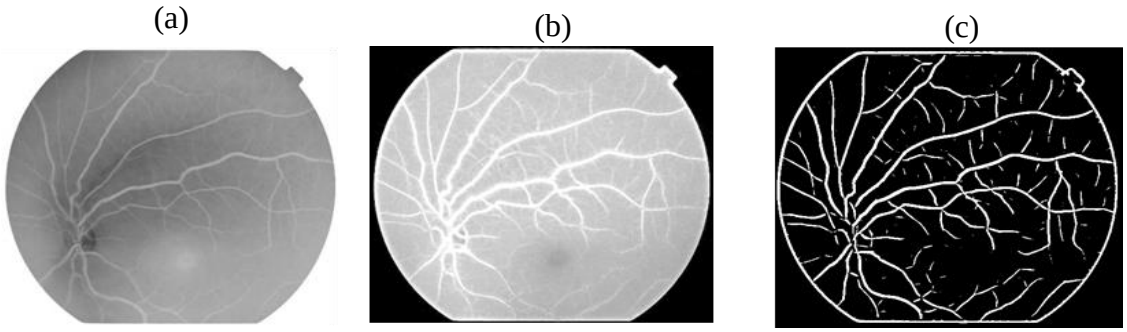

Figure 4-9 (a) the Green inverted image (b) wavelet based enhanced vascular tree (c) Separated Vascular Network

Morphological Operations

The next stage is to remove the mask boundary and the small spurs that are not connected to the vascular tree so that we have one whole connected component.

This is done through morphological operations in the following order

1. An erosion to remove the circular boundary.
2. Closing to reconnect the disconnected parts
3. Area based opening that removes all spurs that were present and had appeared as a result of the closing operation.

The three steps are shown in figure 4.10 below:

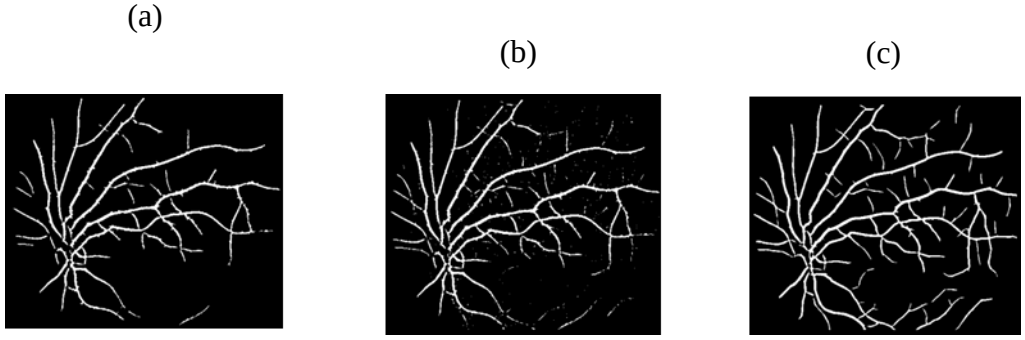

Figure 4-10 (a) removing the circular boundary (b) morphological closing (c) removing small spur

Figure 4- 11 shows images from the local database and their extracted vessel mask.

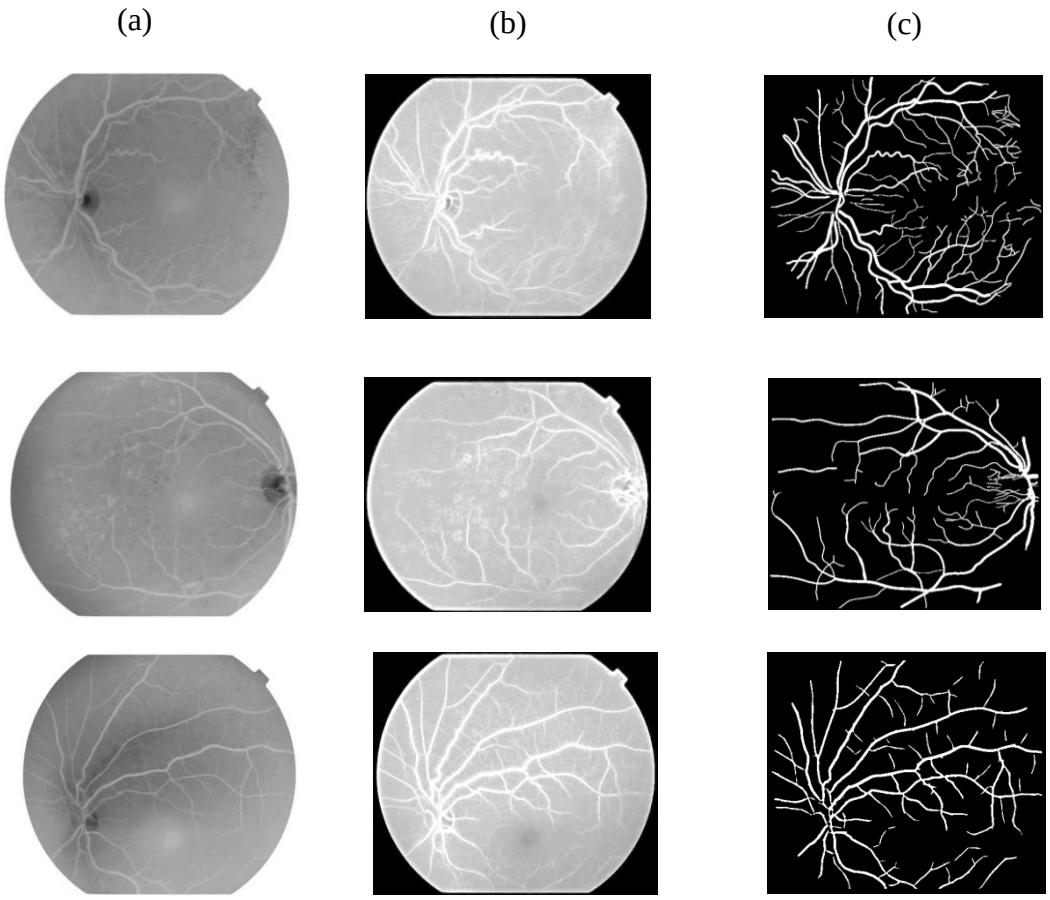

Figure 4-11 (a) Green channel image (b) wavelet vessel enhancement (c) extracted Vessel tree

4.1.3. Skelotonisation and Bifurcation points

Now that we have the vascular mask, our primary goal has been achieved. To be able to process the tree, we need to separate the vessel segments. To achieve this, we require two steps:

1. **Skelotonisation**: is a morphological operation where the algorithm starts thinning the vessels iteratively while keeping it intact till there is no change between two consecutive images. Figure 4.12 shows a few iterations and the final result.
2. **Determining the Branch points**: A branch point is a point where two or more vessels meet. A pixel is defined as a bifurcation or branch point if in a 3x3 neighborhood, five or

more pixels are on or the sum of pixels is equal to two. Any pixel meeting the criteria is removed from the vascular tree. Mathematically,

$$CN = 0.5 \sum_{i=0}^{8} |P_i - P_{i+1}| \; P_9 = P_1 \tag{4.8}$$

Where CN = 2 means a branch point and CN=3 means a bifurcation [33]. Figure 4.13 displays all the detected branch-points and bifurcations.

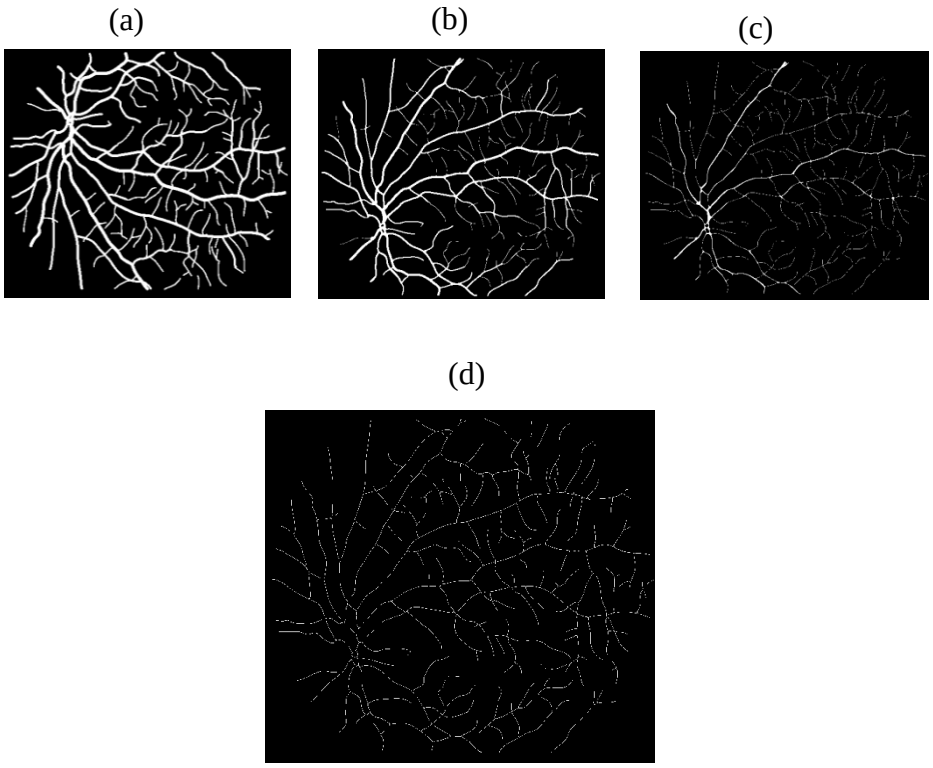

Figure 4-12 Skelotonisation (a) Original Vessel mask (b) After 2 iterations (c) After 5 iterations (d) Vessel skeleton

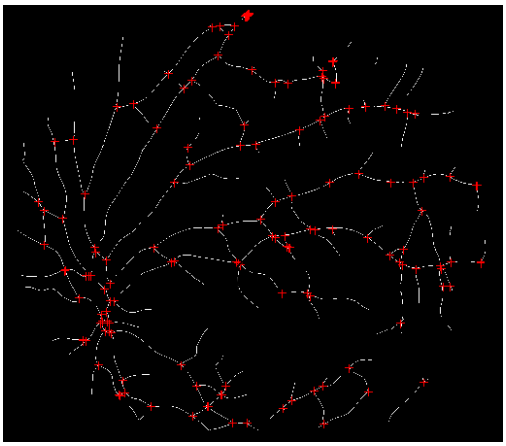

Figure 4-13 Branch points on the vessel tree marked with red-cross.

4.1.4. Seperated Vessel Segments

After the bifurcation points are removed, the vascular tree has now turned in to a number of vessel segments. This yeilds many small segments too. Only those with significant lengths are used for further processing. In our case, Morphological opening is done to remove vessel with samller areas. Aditionally, those with a perimeter greater than the mean perimeter are retained .Figure 4.14 shows an image with labelled vessel.

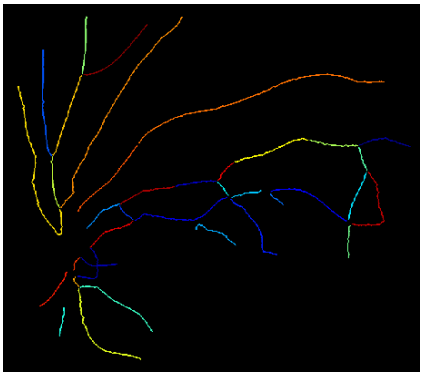

Figure 4-14 Labelled Vessel segments shown in different colors

4.1.5. Feature Extraction

Most of the methods mentioned in literature review use mathematical calculations to identify if the vessel is normal or not. While these may yield highly accurate results, they inflict a heavy computational burden. Our aim in this methodology is to find a computation-accuracy balanced approach. The features used here are motivated from appearance of tortuous vessels. Compared to normal vessels, tortuous vessels have more bends, curvature, irregularity in gradient flow etc. A feature set is proposed in this research to accommodate all these changes. The proposed features belong to three categories: i) Structure based features ii) Peak based features and iii) Gradient based features.

Structure based features

1. **Tortuosity**

Tortuosity is how twisted a curve is or how many numbers of turns it has. Here we use the basic formula proposed by Lotmar et al [16] to calculate the tortuosity of each vessel segment, that is:

Tortuosity = Arc length / chord length

Where Arc length is basically the perimeter of the vessel and chord length is the Euclidean distance between the endpoints. Figure 4.15 shows vessels with different tortuosity values:

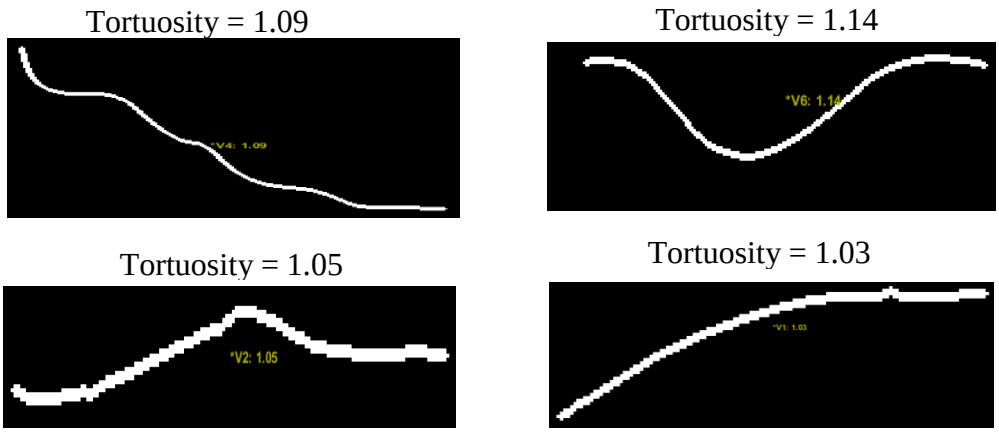

Figure 4-15 Vascular Segments with different tortuosity

The curves shown in figure 4-15 give a clearer idea; the second vessel has the highest tortuosity value owing to the most angular bend. The first one looks considerably straight but has a larger value because of its larger perimeter.

Although this formula is the most robust method yet as termed by [19] but it has a drawback in that it cannot differentiate between a large tortuous curve and a very small curve with a high angular bent. Hence more features are needed to support classification.

2. Aspect Ratio

Aspect ratio is the ratio of the Major Axis length to the Minor Axis length of the ellipse that best fits a curve, expressed as

Aspect ratio = Major Axis length of the fitted ellipse/ minor Axis length (4.9)

The value ranges from a 0 for straight lines to 1 for a circle. The idea here is that a vessel with significant bending will have a larger minor axis length and hence a smaller aspect ratio. Through testing, an empirical value of 10 was selected to further filter the vessel segments that passed a certain length.

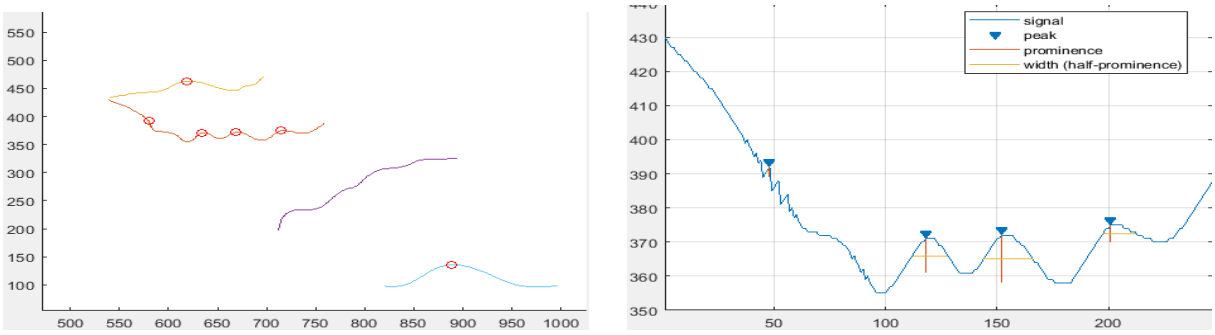

Figure 4-16 (a)Peaks detected for each vascular segment marked with red circles (b) Peak width (yellow horizontal line) and Peak prominence (red vertical line)

Peak based features

3. Number of Peaks

An abnormal vessel becomes more twisted, this mean an increase in the number of peaks compared to a normal vessel. A pixel is a peak pixel if it has a large value compared to its neighboring pixels or has a value of infinity.

4. Peak Width

The vessels have a characteristic curvy shape. Due to this reason not all peaks are true peaks. For a tortuous vessel, a peak appears after approximately 5 to 10 pixels or more and not after every other pixel. So to cater this, peak width is determined to add clarity to the number of peaks. Tortuous vessels normally have low peak width when compared to normal ones.

5. Peak Prominence

Peak prominence refers to the amplitude of each peak measured from the previous neighboring pixel. Since we want to detect significant bents only, peak prominence completes the criteria for peak selection. Only peaks greater than 3 pixels are categorized as peaks. Figure 4-16 displays detected peaks on a few vessels and also the peak prominence and peak width. Notice how there are no peaks detected for the purple labeled segment, since only those with a Height greater than 3 pixels are to be counted.

Gradient based features

6. Mean of Gradient Magnitude

A Gradient of the image gives the location of edges in the image in terms of their distance and angular direction from each pixel. A gradient image was taken of the original gray image using

the Sobel operator and the mean value of all the magnitudes of each labeled segment calculated using the usual formula:

$$\text{Mean magnitude, Xm} = (\sum X_i)/n_p \quad (4.10)$$

Where Xi is the gradient magnitude at the i-th pixel of the vessel segment and n_p is the total number of pixels in that segment

Figure 4-17 shows the gradient image of both direction and magnitude. The length of the arrows in figure 4-17 (b) gives its magnitude at that location and the direction tells the phase.

(a)

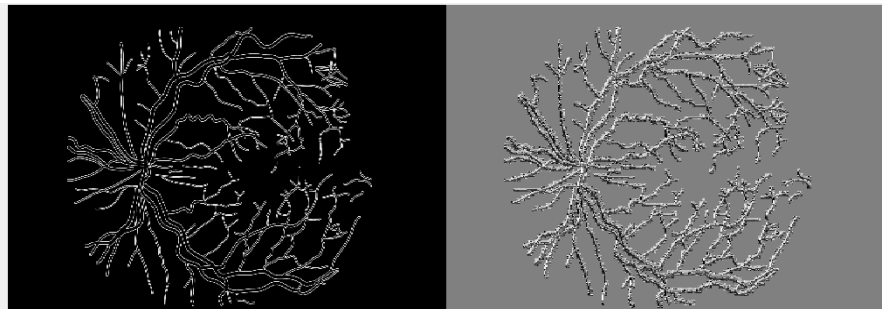

(b)

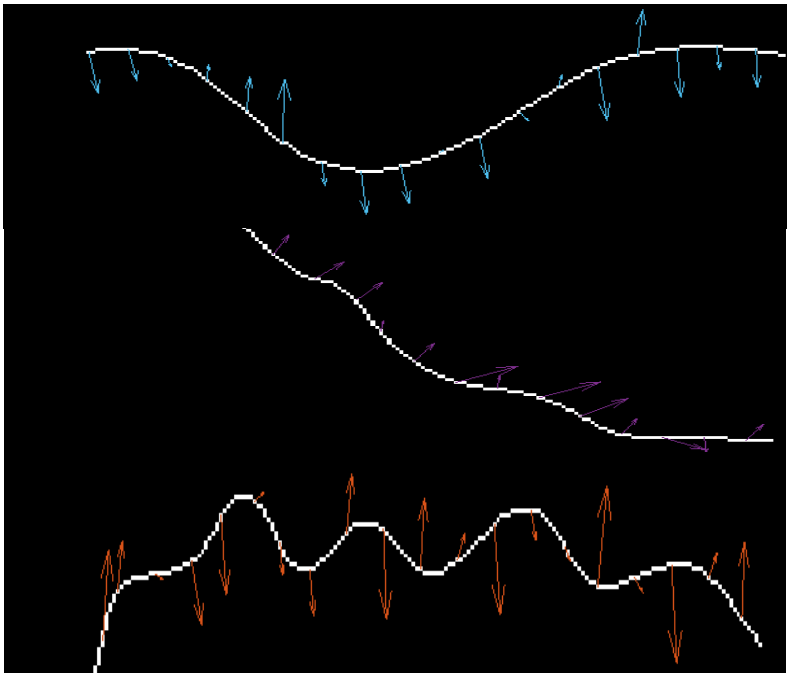

Figure 4-17 (a) shows the gradient magnitude (L) and direction images (R), (b) arrows showing the magnitude and direction of vessel segments

It is clearly seen that, the last vessel is a tortuous vascular segment and shows additional number of direction changes compared to the other two segments.

7. Standard deviation of Gradient Magnitude

Next the standard deviation was calculated for each set to determine the spread or the change in the data. An abnormally tortuous vessel would have a higher standard deviation compared to the other vessels because there are a greater number of significant angular changes. The standard deviation is given by

$$std = \sqrt[2]{\sum(X_i - X_m)/n_p} \tag{4.11}$$

Where Xi is the gradient magnitude at the ith pixel of the vessel segment, Xm = mean of the data and n_p = total number of pixels in that segment

8. Mean of Gradient phase

This is the mean of phase values obtained from the gradient image for each vessel segment. Gradient phase gives us the angular direction in radians of the location of the edge nearest to that pixel. The directional vectors on blood vessel segments are shown in figure 4.17(b).

9. Standard Deviation of Gradient phase

The standard deviation is calculated using equation 4.11 with the phase values and phase mean. The higher the standard deviation of phase, the greater the number of phase changes. Thereby, indicating a tortuous vessel.

4.2. Classification

We use support vector machines (SVM) to detect the tortuous vessels in an image. Since equal number of samples are not present for the normal and abnormal vessels, we use a one class support vector machine (OC-SVM) for classification.

One Class Support Vector Machines

Support vector machine (SVM) is a supervised machine learning tool. It builds a classification model on a given training set and uses it to classify or predict labels for a new set. Figure 4-18

shows a linear SVM that separates the data using a linear function. It classifies objects based on a ‘maximum margin ’approach. That is the data is mapped in to space where it is divided into two or more classes based on a hyper plane that gives the maximum margin between the two classes while minimizing the generalization error. SVMs have the ability to resolve non- linear issues. They uses various kernel functions to project the data in to a higher dimensional space where the classes can be separated by a linear boundary. Functions that define the boundaries in the linear space include the Gaussian or RBF kernel, sigmoid, and the polynomial kernel where the boundary is defined by the best minimum order polynomial.

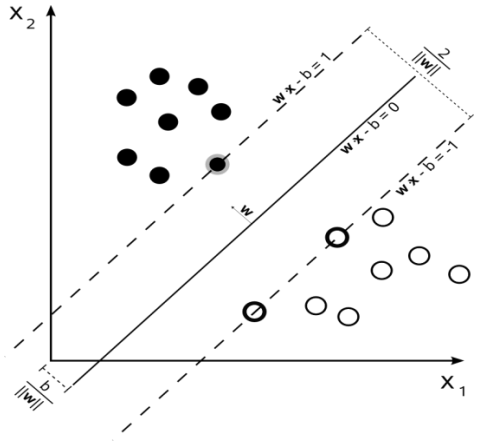

Figure 4-18 Linear SVM model for two classes- the chosen hyper-plane gives the maximum distance between the two classes. Points lying on the dotted lines are called support vectors [34]

Figure 4-19 a- d shows steps in determining the best hyper-plane to classify the data. As shown in (a) three hyper planes A, B, C are determined but only B separates the data completely. Where there are multiple choices for the boundary as in (b), the one which maximizes the margin between the nearest data points is selected. From A, B, C- C shows the maximum margin from the nearest data point. Hence C would be the correct choice. In (c) B is chosen as the best hyper-plane because it effectively separates the two classes.

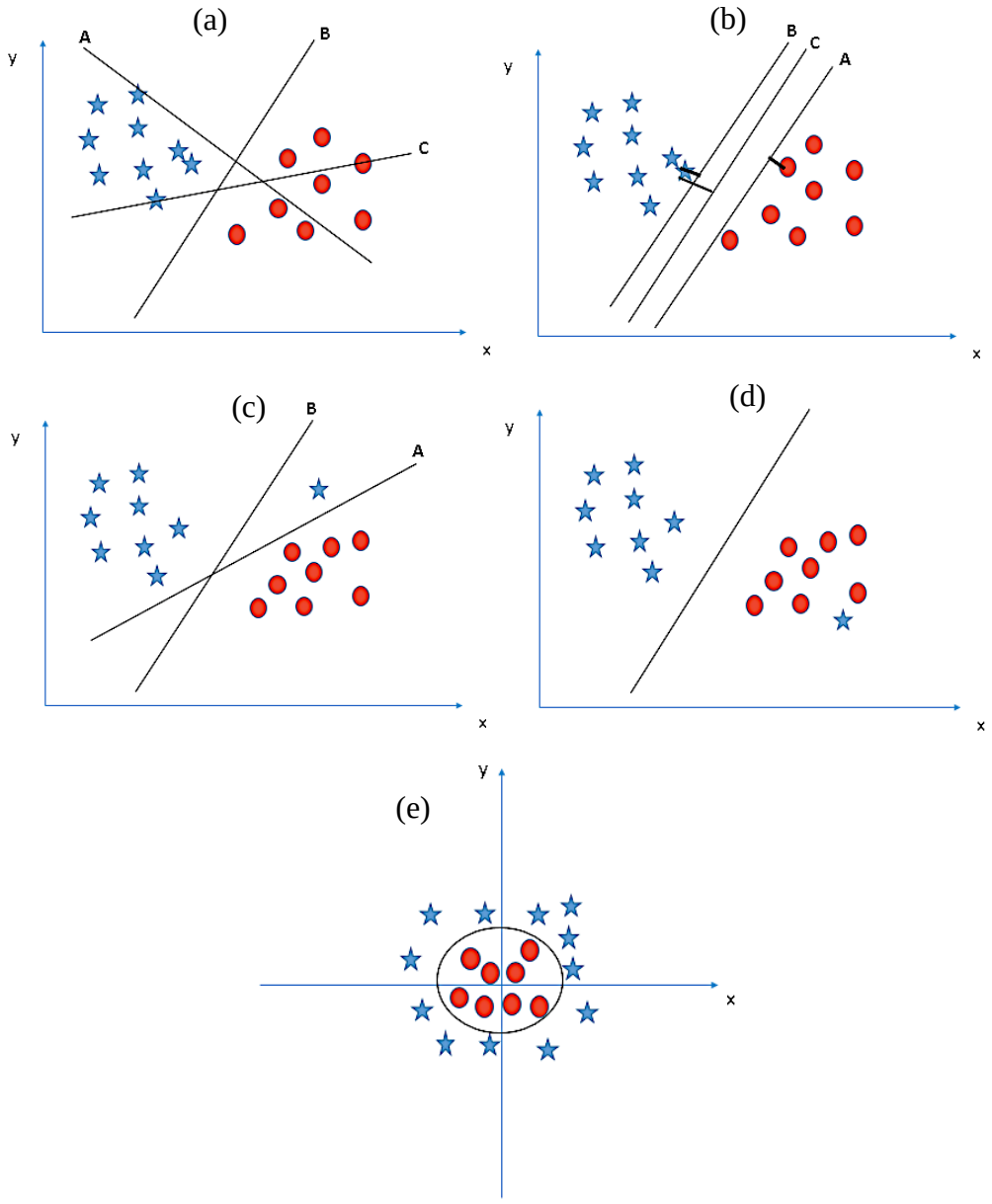

Figure 4-19 Hyper-plane examples for different data scenarios in SVM [35]

One class SVMs are used for anomaly detection or where there is an abundance of one class of data compared to the other. Origin is considered as the only point from the anomaly class and a plane is formed which maximizes the distance between the given data and the origin. The Gaussian or RBF kernel, is a popular choice for one class SVM and usually results in a circular separation boundary as shown in figure 4.19 (e). Figure 4.20 shows the contours that were used to detect the boundaries. The maximum margin boundary is where the contour is equal to 0.

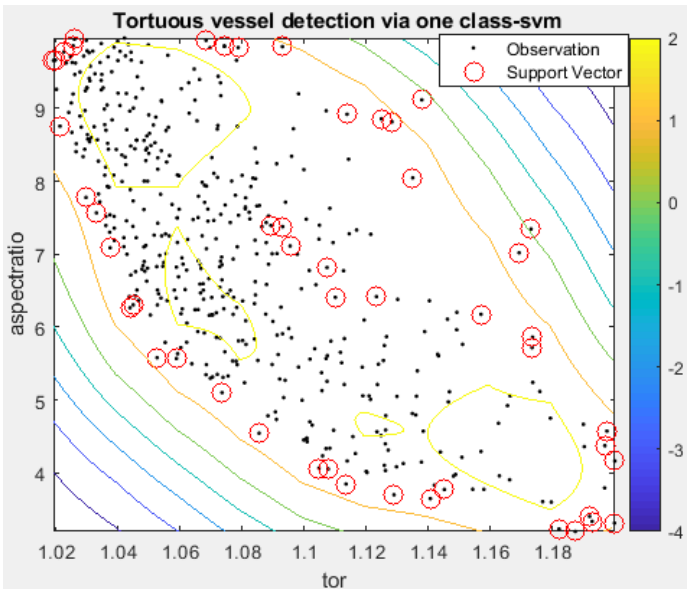

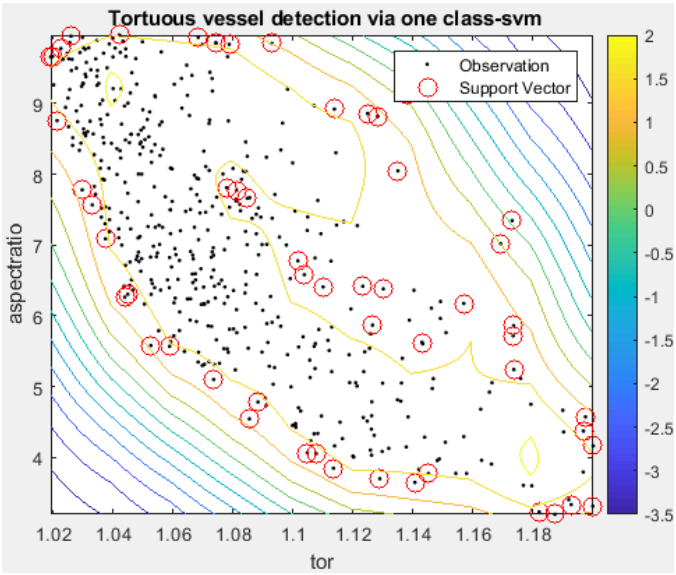

Figure 4-20 one class SVM model

Now, that vessel are obtained from each fundus image and features are extracted, the SVM model is evaluated on some primary parameters for results.

5. Experimental Results

5.1 Dataset and specifications

The proposed algorithm was tested on a local dataset obtained from Armed Forces Institute of Ophthalmology (AFIO), Rawalpindi, Pakistan. The dataset has 100 RGB fundus images of size 1000x1504 saved as JPEG files. The dataset contains manually segmented vessels, arteries & veins masks. Annotation for vessel segments being normal or tortuous is also done for the dataset. Figure 5-1 shows a few images from the dataset.

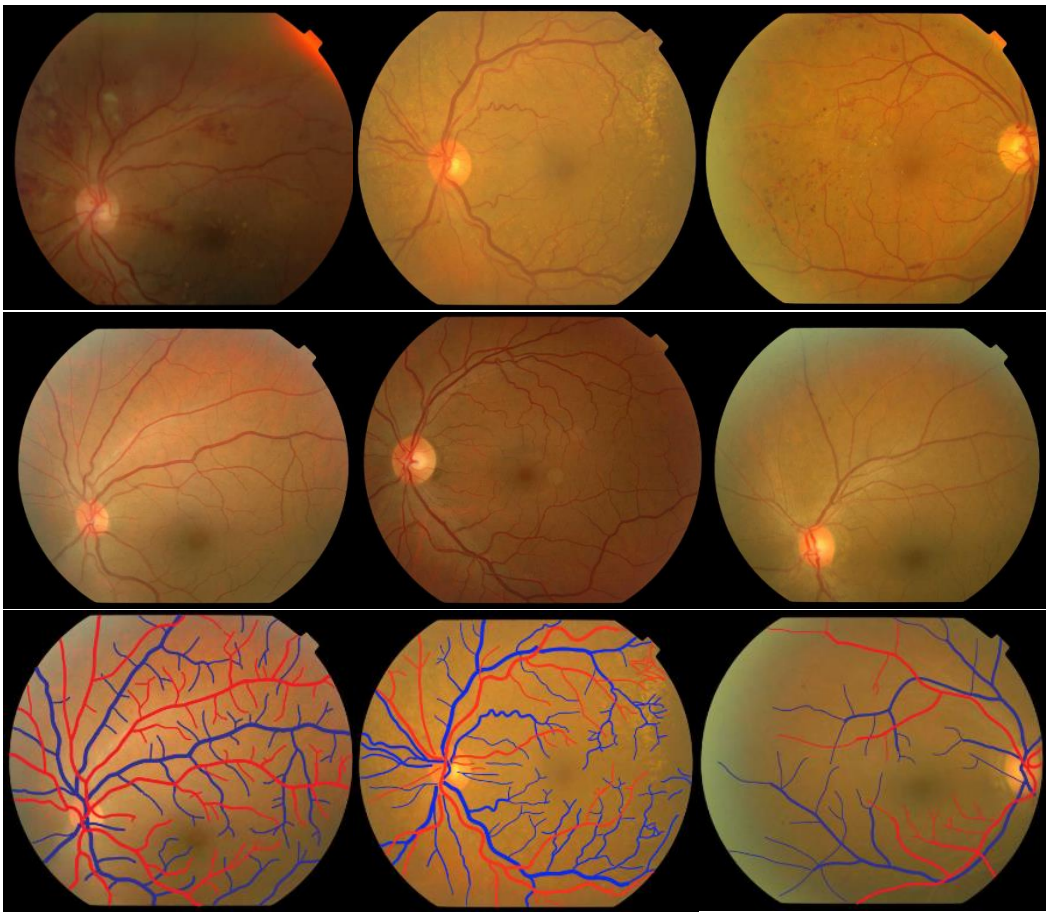

Figure 5-1 Images from local dataset, [3rd row] shows arteries (red) and veins (blue)

The given methodology extracted a total of 757 combined blood vessel segments from these images of which 163 were tortuous. As per the rule, binary SVMs work better when there are equal samples of both the classes present but our data is not structured as such. So, One-class Support Vector Machine (OC-SVM) was used with the default Gaussian kernel and nu set to

0.09 for an optimum result. Moreover, nine features (Tortuosity, number of peaks, mean peak width, mean peak prominence, mean gradient magnitude, standard deviation of gradient magnitude, mean gradient phase, standard deviation of gradient phase, aspect ratio) were calculated for each blood vessel segment which gave us a reasonably sized feature vector of 757x9. The data was divided in to 60:40 ratio (~ 475:282 vessel segments).

The same methodology and SVM model was used to segment and classify arteries and veins separately. A total of 239 arteries were separated of which 44 were tortuous and 351 vein segments were formed of which 83 were tortuous.

The tortuous vessel segments form our positive class and are labelled as 0 while the normal vessels are labelled as 1.

Figure 5-2 displays scatter plots of a few combinations of the features for the combined vessels. Testing was done on multiple combinations of feature set but only those with two features are shown.

1.Tortuosity vs. aspect ratio

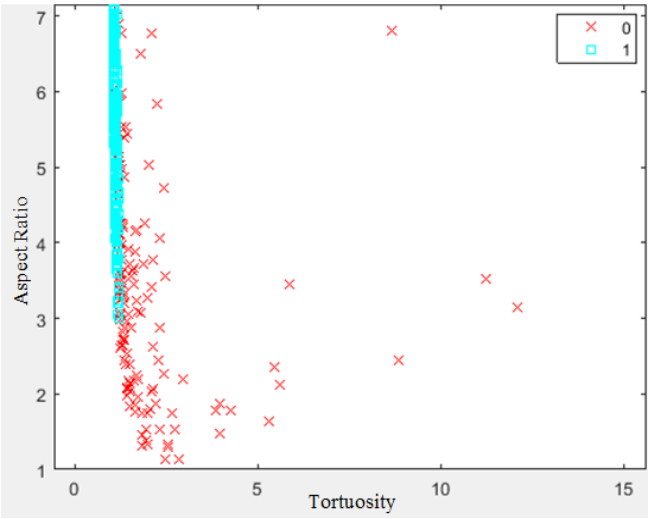

2. Tortuosity vs. number of peaks

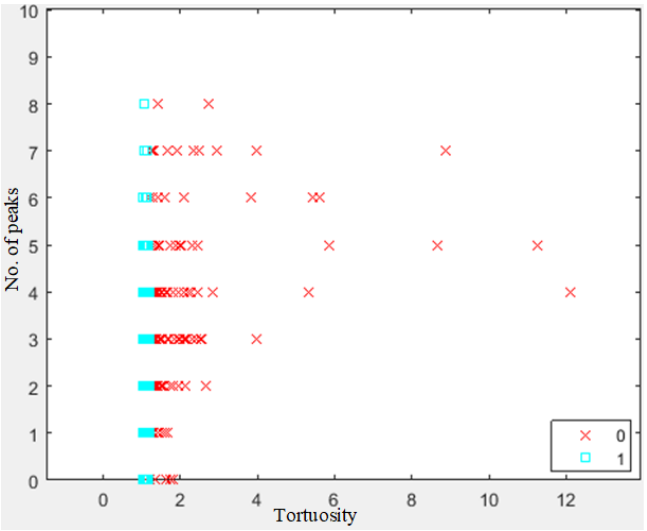

3.Tortuosity and std gradient phase

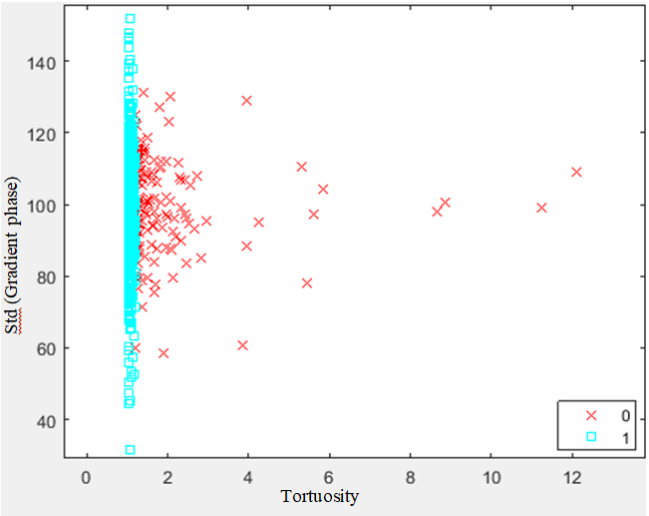

4.Number of peaks and std gradient phase

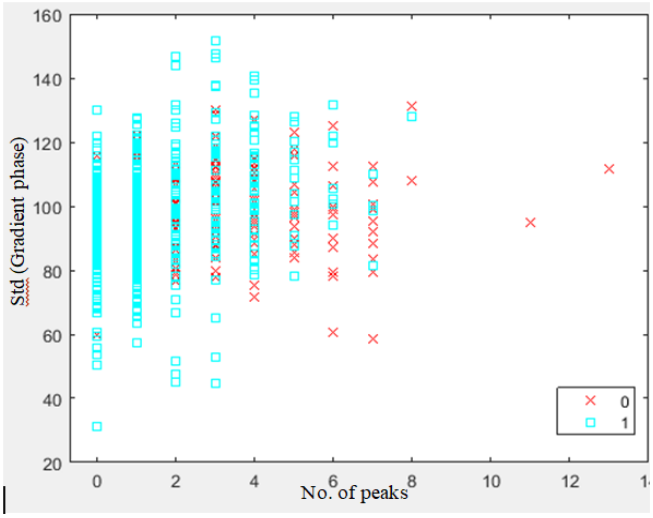

5. Std Gradient phase vs mean peak prominence

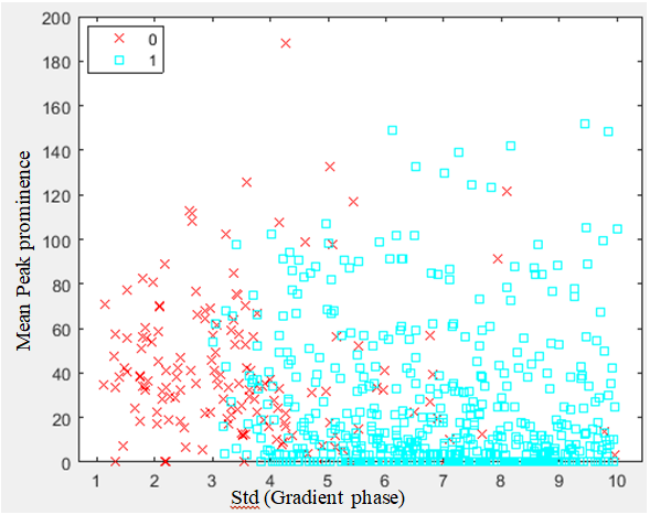

Figure 5-2 Scatter plot of Features (xvars vs yvars), cross= Class 0 (tortuous vessels), square = class 1(normal vessels)

Scatter plots show how separable in space the data is. For instance, in the last scatter plot, the tortuous vessels (cross) have a low aspect ratio and mean peak prominence. Most of the normal vessels (square) have a comparatively higher aspect ratio with low mean prominence. For one class SVM, 60 percent of the normal vessels were used for training while the rest of the data was used for testing. The model was tested with

1. Individual features
2. The whole feature set
3. A few combinations of the features

Figure 5-3 shows scatter plots for arteries and veins.

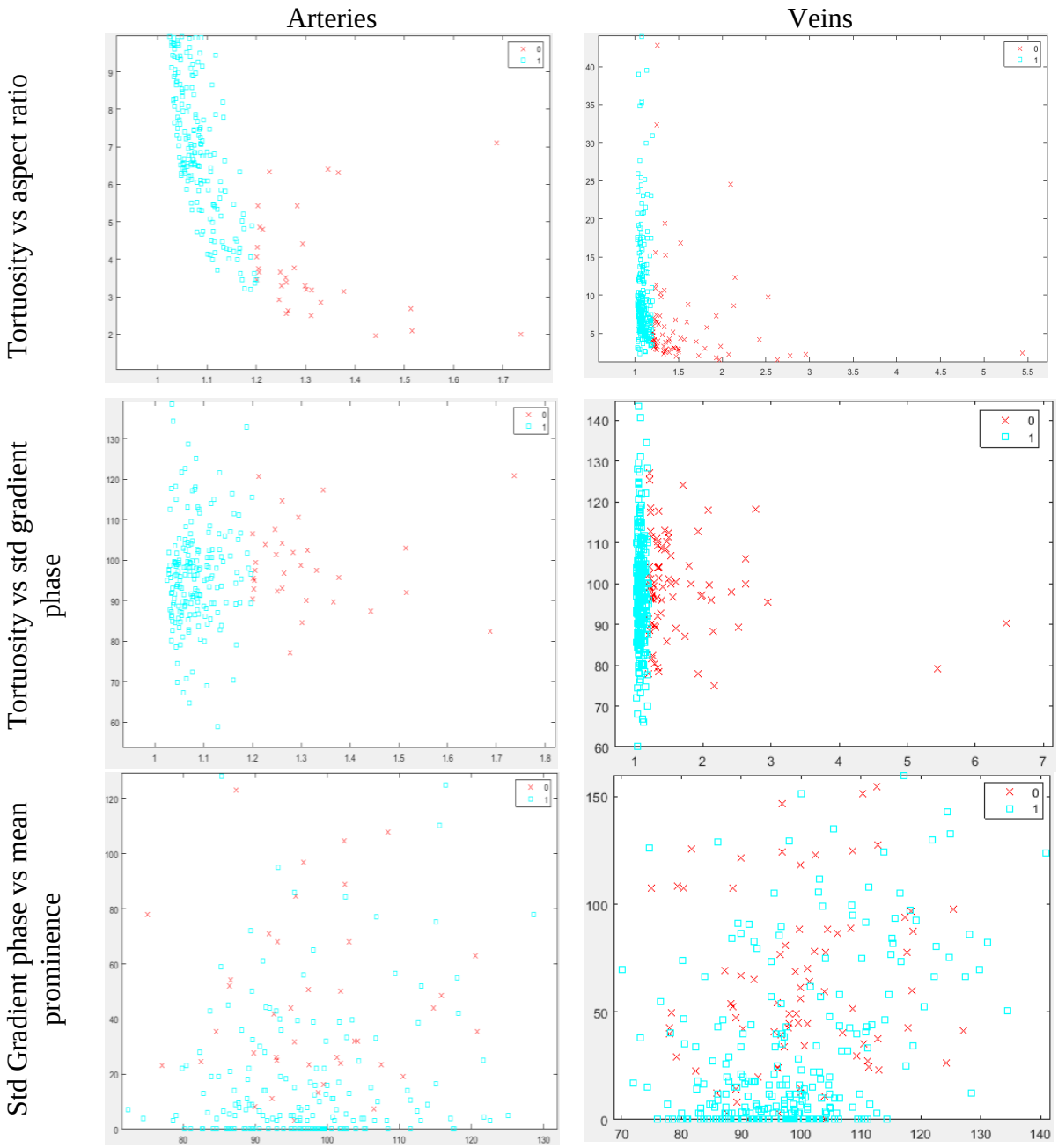

Figure 5-3 Scatter plots showing distribution of samples for arteries and veins (xvar vs yvar), cross = Class 0 (tortuous vessels), square = class 1(normal vessels)

5.2 Performance Measures

The common parameters for evaluation of the results are sensitivity (SEN), specificity (SPE), and accuracy (ACC). Another measure is the Receiver Operating Curve (ROC), obtained by plotting True Positive Rate (TPR) against False Positive Rate (FPR) that gives Area under the curve (AUC), where the maximum value for AUC is 1. Mathematically,

$$SEN = TPR = \frac{TP}{TP + FN} \tag{5.1}$$

$$SPE = TNR = \frac{TN}{TN + FP} \tag{5.2}$$

$$ACC = \frac{TP + TN}{TP + TN + FP + FN} \tag{5.3}$$

Where in classification,

TP = number of abnormal or tortuous retinal vascular segments correctly classified as abnormal

FP = number of normal vessel segments wrongly classified as tortuous.

TN = number of normal vessel segments correctly classified as normal

FN = number of tortuous vessels wrongly classified as normal.

5.3 Results

Table 5-1, 5-2 and 5-3 show results for above mentioned performance measures for combined vessels, arteries and veins, respectively. The values of specificity, sensitivity and accuracy are listed against the features used to build the SVM model for that particular vessel type. Specificity in the table refers to the detection of label 1 as a 1, it has the maximum results because the classifier was trained on this class and therefore can show the best response towards it. Arteries show the lowest sensitivity because of the scanty presence of tortuous arteriolar segments. The model giving the best accuracy for each vessel type is in bold in the table.

Table 5-1 : Performance measures of different feature combinations for one class svm for combined vessels

Features	Sen	Spe	Acc(%)	Features	Sen	Spe	Acc(%)
Tortuosity	0.9080	1	94.70	Tortuosity and aspect ratio	**0.8773**	**0.9177**	**92.6**
Number of peaks	0.0245	1	43.83	number of peaks, peak width, peak prominence,	0.01227	1	43.11
Mean Peak width	0	1	42.40	Mean Gr. Mag, Std Gr,Mag, Mean Gr.phase, Std Gr.	0.01277	1	43.11
Mean Peak prominence	0.0061	0.9917	42.4	Tortuosity, number of peaks, mean gradient magnitude, mean gradient phase	0.7914	1	88
Mean(Gradient magnitude)	0.0245	1	43.82	Tortuosity, number of peaks, std gradient phase, aspect ratio	0.8344	1	90.5
Std(Gradient magnitude)	0.0184	0.9917	43.11	Tortuosity, number of peaks, peak width, peak prominence, Aspect ratio	0.7669	1	86.57
Mean(Gradient phase)	0.0061	0.9917	42.40	Tortuosity, std gradient, aspect ratio	0.8466	1	91.2
Std(Gradient phase)	0	1	42.40	Tortuosity and number of peaks	0.9448	0.8000	88.3
Aspect Ratio	0.4540	0.9750	67.49	Tortuosity and std gradient phase	0.8405	1	90.8
All the above features	0.7791	1	87.28	Std gradient phase and mean peak prominence	0.3681	1	63.6

Table 5-2 Performance measures of different feature combinations for one class svm for Arteries

Features	Sen	Spe	Acc(%)	Features	Sen	Spe	Acc(%)
Tortuosity	1	1	100	Tortuosity and aspect ratio	**0.8636**	**1**	**97.49**
Number of peaks	0.09090	0.995	82.845	number of peaks, peak width, peak prominence,	0.0454	1	82.427
Mean Peak width	0.02272	0.974	79.92	Mean Gr. Mag, Std Gr,Mag, Mean Gr.phase, Std Gr.	0.0227	1	82.008
Mean Peak prominence	0.02272	0.995	81.59	Tortuosity, number of peaks, mean gradient magnitude, mean gradient phase	0.7727	0.995	95.397
Mean(Gradient magnitude)	0.02272	0.9744	79.916	Tortuosity, number of peaks, std gradient phase, aspect ratio	0.8181	0.985	95.397
Std(Gradient magnitude)	0.02272	0.995	81.59	Tortuosity, number of peaks, peak width, peak prominence, Aspect ratio	0.8409	0.985	95.816
Mean(Gradient phase)	0	1	81.59	Tortuosity, std gradient, aspect ratio	0.8181	0.995	96.234
Std(Gradient phase)	0.02272	1	82.008	Tortuosity and number of peaks	**1**	0.877	89.958
Aspect Ratio	0.45455	0.995	89.54	Tortuosity and std gradient phase	0.8409	0.995	96.653
All the above features	0.7500	0.990	94.56	Std gradient phase and mean peak prominence	0.0227	1	82.008

Table 5-3 Performance measures of different feature combinations for one class svm for Veins

Features	Sen	Spe	Acc(%)	Features	Sen	Spe	Acc(%)
Tortuosity	1	1	100	Tortuosity and aspect ratio	**0.9518**	**0.993**	**98.291**
Number of peaks	0.0964	0.989	77.78	number of peaks, peak width, peak prominence,	0.0843	0.996	78.063
Number of peaks	0	0.993	75.78	Mean Gr. Mag, Std Gr,Mag, Mean Gr.phase, Std Gr.	0.0241	0.993	76.353
Mean Peak width	0.0241	0.993	76.35	Tortuosity, number of peaks, mean gradient magnitude, mean gradient phase	0.8192	0.787	79.487
Mean(Gradient magnitude)	0	0.993	75.783	Tortuosity, number of peaks, std gradient phase, aspect ratio	0.9277	0.728	77.493
Std(Gradient magnitude)	0.0241	0.993	76.353	Tortuosity, number of peaks, peak width, peak prominence, Aspect ratio	0.8192	0.757	77.208
Mean(Gradient phase)	0.0120	0.996	76.353	Tortuosity, std gradient, aspect ratio	0.8795	0.716	75.499
Std(Gradient phase)	0.0361	0.989	76.353	Tortuosity and number of peaks	0.9759	0.944	95.157
Aspect Ratio	0.4819	0.705	65.242	Tortuosity and std gradient phase	0.8554	1	96.581
All the above features	0.8193	0.993	95.157	Std gradient phase and mean peak prominence	0.0241	0.993	76.353

An optimization technique for SVMs is to build a model with minimum number of features that separates the classes well without compromising the original accuracy. It can be seen that, SVM model built on structural features, tortuosity and aspect ratio, gives the maximum accuracy for all three data sets and best sensitivity for combined vessels and veins. The results also show that feature reduction while keeping those that separate the class optimally shows an increase in accuracy and an inevitable reduced computational load.

Contour plots for SVM models based on two features (selected from the table) are shown below in figure 5-4:

1. Tortuosity and aspect ratio

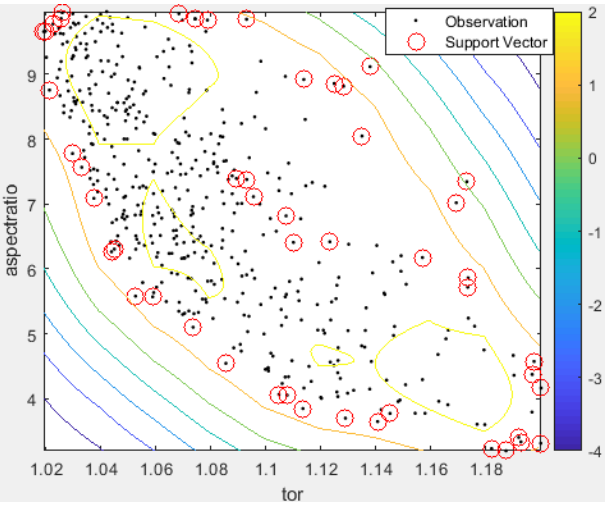

2. Tortuosity and number of peaks

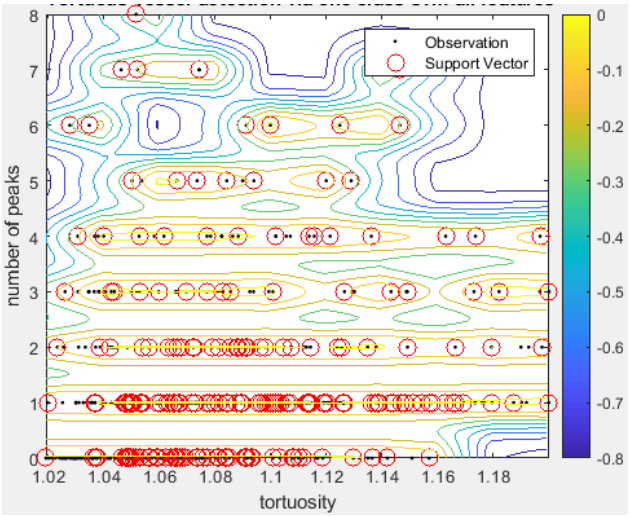

3. Tortuosity and std gradient phase

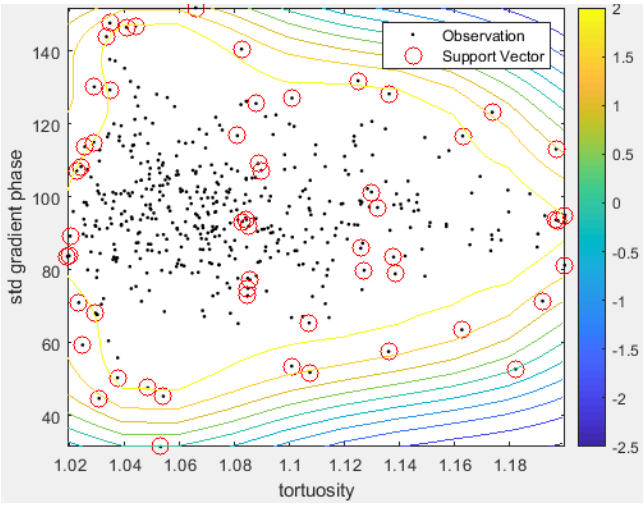

4. Number of peaks and std gradient phase

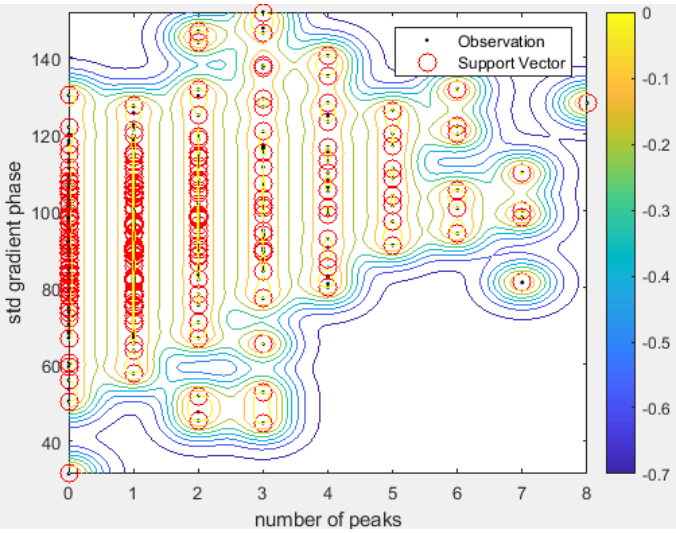

5. Std Gradient phase and mean peak prominence

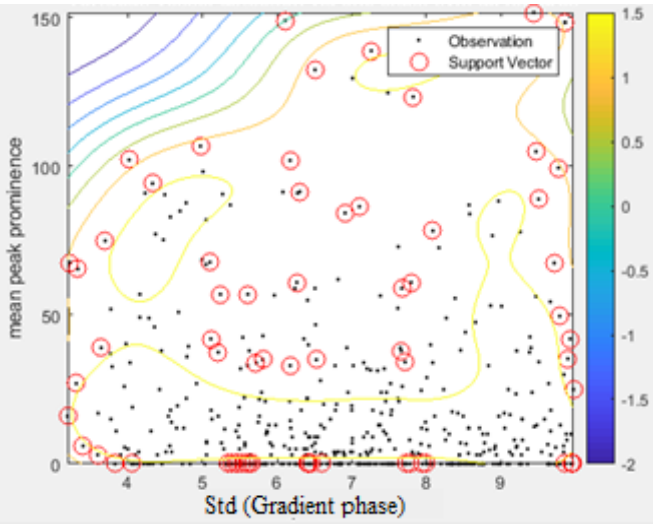

Figure 5-4 Contour plots showing SVM boundary

The contour plots also confirm the accuracy results. Poorly formed models lead to a very low accuracy of 53% as shown in the 4th model of figure 5-4. Model 2 is giving a good accuracy of 88% but shows over fitting in that all samples are being used as support vectors.

Figure 5-5 shows the Receiver Operating Curves (ROC) for SVM models built according to the three feature categories (structural, peak based, gradient based), with the Area under the curve (AUC) stated for that model. Hence, confirming results from the table.

Figure 5-6 also shows ROCs for 6 randomly selected SVM models from the table, for each vessel type.

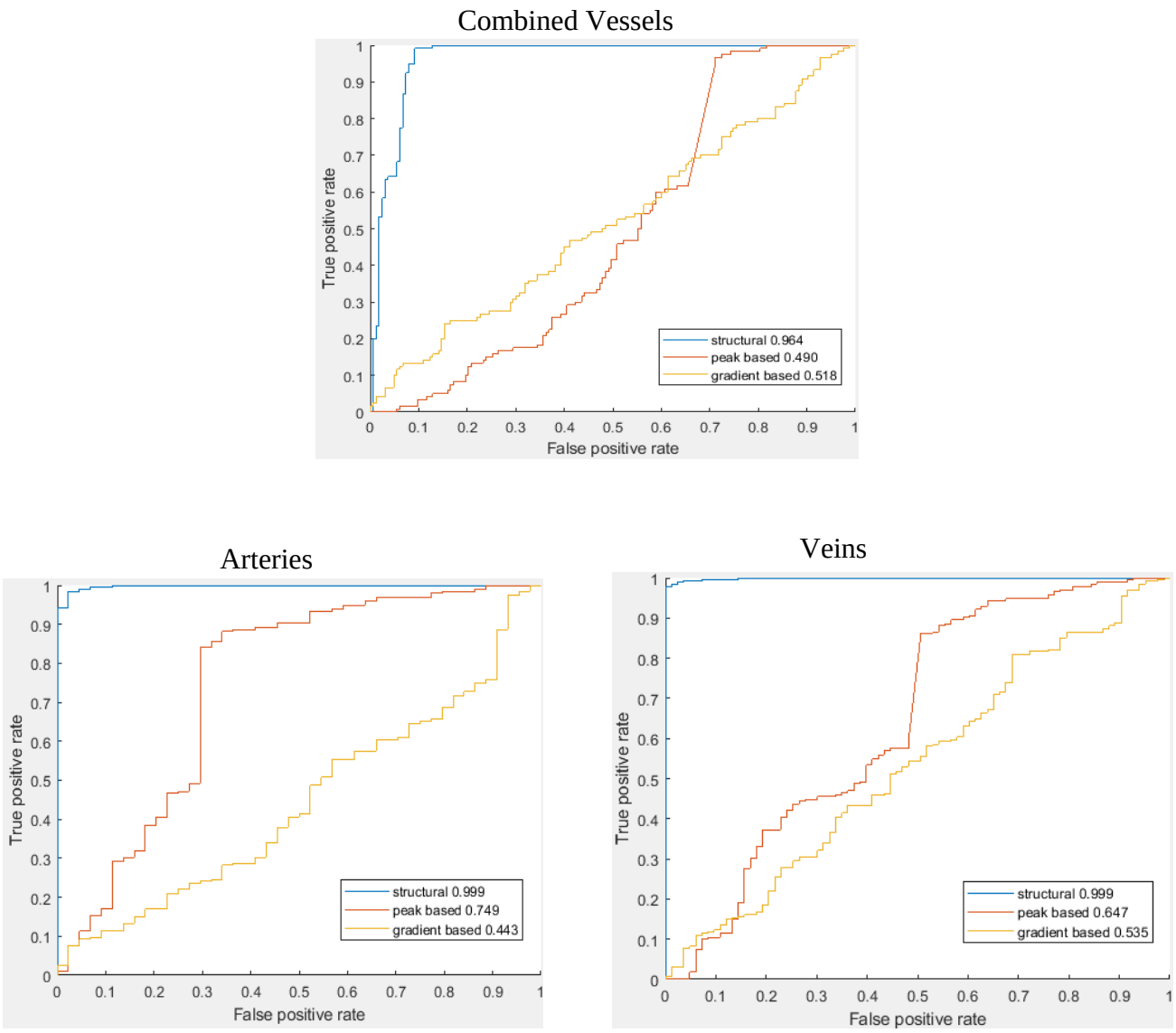

Figure 5-5 Receiver Operating Curves (ROC) for the three feature categories, for each vessel type.

Combined vessels

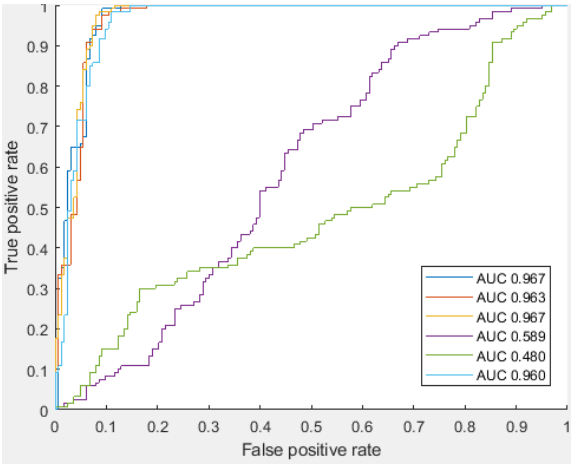

Arteries

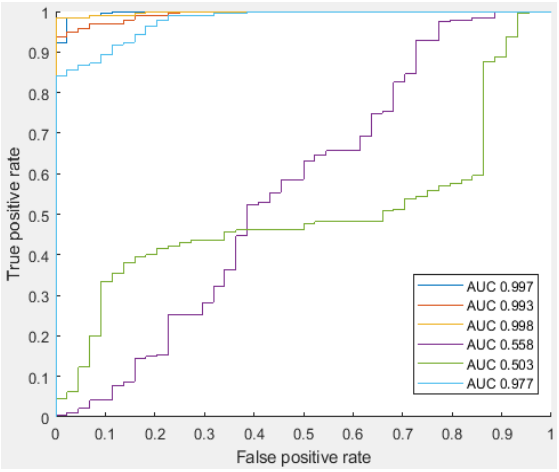

Veins

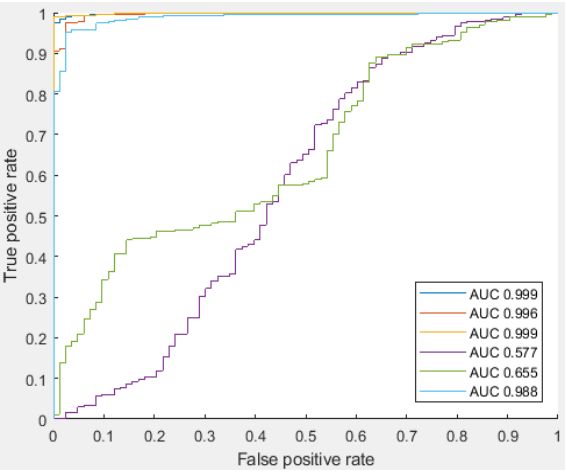

Figure 5-6: ROC curves for 6 random iterations for Combined Vessels, Arteries and Veins

All the vessel segments from an image are passed to the SVM model which predicts labels for the new segments. Normal and tortuous vessels are displayed in different color each, for all three experiments as shown in the figure 5-7 below.

Combined vessels

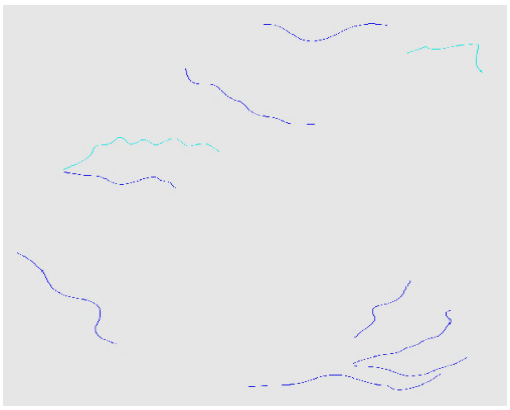

Arteries

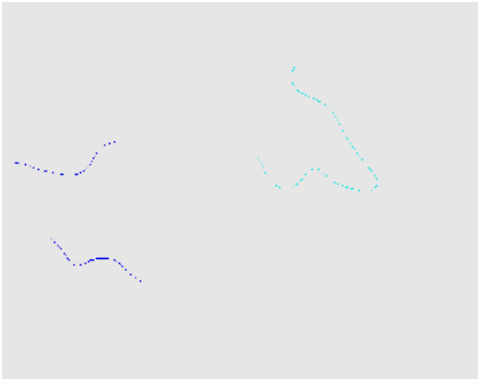

Veins

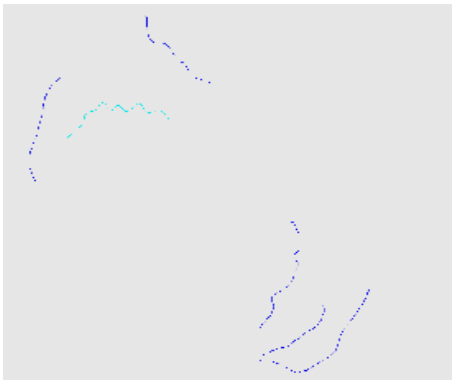

Figure 5-7 Predicted Labelled Vessels, Light blue = Tortuous vessels, Dark blue = Normal vessels

6. Conclusion and Future Work

6.1 Conclusion

New Healthcare studies have ranked high consumption of sugar as the leading risk factor to human health. Consequently, it is vital to maintain a balanced blood sugar level. Unstable sugar levels can lead to Diabetic retinopathy. Though potentially hazardous, DR can be detected using fairly non-invasive techniques, for instance analysis of fundus images.

The results show that automatic classification of vessel segments as tortuous or normal in ocular fundus images is possible through OC-SVM, which proved to be a suitable tool for classification with an accuracy of 87%., 94% and 79% for combined vessels, arteries and veins respectively. Minimizing the number of features further improved the accuracy of the SVM models to 93% for combined vessels and 97%, 98% for the latter two.

6.2 Contribution

- A new hybrid feature set for detection of vessel tortuosity
- Fully automated system for segmentation and classification of vascular tortuosity from colored retinal fundus images
- Review of mathematical approaches to determine tortuosity of retinal vessels.

6.3 Future Work

Owing to its impact on an individual's life, DR is a critical research area. In future, the dataset can be improved to have more tortuous vessels. This is important to have good modelling of tortuosity. Also further detection and classification of IRMA can be done. Additionally, the algorithm can be tested on various publicly available datasets.

References

[1] C. Mathers and D. Loncar, "Projections of Global mortality and Burden of Disease from 2002 to 2030," *PLoS Medicine,* vol. 3, no. 11, p. 442, 2006.

[2] N. Congdon, Y. Zheng and M. He, "The worldwide epidemic of diabetic retinopathy," *Indian Journal of Opthalmology,* vol. 60, no. 5, p. 428, 2012.

[3] V. Joshi, C. Agurto, R. VanNess, S. Nesmeth, P. Soliz and S. Barriga, "Comprehensive Automatic Assesement of Retinal Vascular Abnormalities for comouter-assisted retinopath grading," *The 36th Annual International Conference of the IEEE,* pp. 6320-6323, 2014.

[4] J. Garvin, 2013. [Online]. Available: http://ffden-2.phys.uaf.edu/211_fall2013.web.dir/jessica_garvin/parts_of_the_eye.html . [Accessed August 2017].

[5] D. Darling, "Retina," [Online]. Available: http://www.daviddarling.info/encyclopedia/R/retina.html . [Accessed August 2017].

[6] "Diabetes Mellitus," [Online]. Available: https://en.wikipedia.org/wiki/Diabetes_mellitus. [Accessed August 2017].

[7] D. Maeda, "Diabetic Retinopathy Ocular Disease IV:Dx and Tx of the posterior segment," [Online]. Available: https://www.slideshare.net/dr_munish/lecture-3-diabetic-retinopathy+.

[8] H. Mirzaei, "Diabetic Eye Disease," [Online]. Available: https://www.slideshare.net/hmirzaeee/diabetic-eye-disease-1155305+. [Accessed 2017].

[9] "Guidelines of Diabetic Retinopathy," [Online]. Available: http://mrcophth.com/guidelinesindiabeticretinopathymanagement/index.html.

[10] A. Agarwal, Fundus fluorescein and indocyanine green angiography, N. SLACK, Ed., Thorofare, 2008.

[11] L. Myers, "Diabetic Retinopath: A Clinical Survival Guide," [Online]. Available: https://www.slideshare.net/eyesteve/iowa-rounds-diabetic-retinopathy-eyesteve. [Accessed 2017].

[12] W. L. Roque, K. Arcaro and A.-B. Angel, "Mechanical Competence of Bone: A New Parameter to Grade Trabecular Bone Fragility From Tortuosity and Elasticity," *IEEE Transactions on Biomedical Engineering,* vol. 60, no. 5, p. Pages: 1363 – 1370, 2013.

[13] E. Bullitt, G. Gerig, S. Pizer, W. Lin and S. R. Aylward, "Measuring tortuosity of the intracerebral vasculature from MRA images," *IEEE Transactions on Medical Imaging,* vol. 22, no. 9, pp. 1163-1171, 2003.

[14] R. Sivakumar, V. Veena and R. John, "A Curvature Based Approach for the Automated Screening of Retinopathyof Prematurity in Preterm Infants," *2017 13th International Conference on Signal-Image Technology & Internet-Based Systems (SITIS),* pp. 503-508, 2017.

[15] M. Abdallah, P. A. Hunter and D. B. Al-Diri, "Quantifying Retinal Blood Vessels' Tortuosity," in *Review, Science and Information Conference,* London, 2015.

[16] W. Lotmar, A. Freiburghaus and D. Bracher, "Measurement of vessel tortuosity on fundus pgotographs," *Graefes Arch. Clin. Exp. Opthalmol,* vol. 211, pp. 49-57, 1979.

[17] H. R. Pourreza, M. Pourreza and T. Banaee, "Simple and efficient Method to measure Vessel Tortuosity," in *Computer and knowledge Engineering (ICCKE) 3rd Internationale Conference Publication*, 2013.

[18] F. Ghadiri, H. Pourreza, T. Banaee and M. Delgir, "“Retinal Vessel Tortusoity Evaluation via Circular Hough Transform”," in *Biomedical Engineering (ICBME), 2011 18th Iranian Conference*, 2011.

[19] E. Grisan, M. Foracchia and A. Ruggeri, "A Novel Method for the Automatic Grading of Retinal Vessel Tortuosity," *IEEE Transactions on Medical Imaging,* vol. 27, no. 3, pp. 310-319, March 2008.

[20] M. Aghamohamadian-Sharbaf, H. R. Pourreza and T. Banaee, "A Novel Curvature-Based Algorithm for Automatic Grading of Retinal Blood Vessel Tortuosity," *IEEE Journal of Biomedical and Health Informatics,* pp. 586-595, 2015.

[21] A. Chakaravarty and J. Siwaswamy, "A novel Approach for Qualification of Retinal Vessel Tortuosity using Quadratic Polynomial Decomposition," *ICMIT IEEE,* 2013.

[22] V. V. Makkapati and V. V. C. Ravi, "Computation of tortuosity of two dimensional vessels," in *2015 Eighth International Conference on Advances in Pattern Recognition (ICAPR),* 2015.

[23] E. H. A. S. Nidhal Khdhair El Abbadi, " AUTOMATIC RETINAL VESSEL TORTUOSITY MEASUREMENT," *Journal of Computer Science,* vol. 9, no. 11, pp. 1456-1460, 2013.

[24] E. Bribiesca, A measure of tortuosity based on chainoding, I. d. I. e. M. A. y. e. S. Department of Computer Science, Ed., Universidad Nacional Auto´noma de Me´xico, , 2012.

[25] D. Onkaew, R. Turior, B. Uyyanonvara, N. Akinori and C. Sinthanayothin, "Automatic retinal vessel tortuosity measurement using curvature of improved chain code," in *International Conference on Electrical, Control and Computer Engineering*, 2011.

[26] N. B. A. Mustafa, W. M. D. W. Zaki, A. Hussain and J. C. Hamzah, " A study of retinal vascular tortuosity in diabetic retinopathy," in *2016 International Conference on Advances in Electrical, Electronic and Systems Engineering (ICAEES),*, 2016.

[27] N. Efford, " Digital Image Processing: A Practical Introduction Using JavaTM.," Pearson Education, 2000.

[28] R. Gonzale and R. Woods, " Digital Image Processing," Addison-Wesley Publishing Company, 1992, pp. 81-125.

[29] M. U. Akram and S. A. Khan, "Multilayered thresholding-based blood vessel segmentation for screening of diabetic retinopathy," *Engineering with Computers,* vol. 29, no. 2, pp. 165-173, 2013.

[30] G. Wavelet, "Gabor Wavelet https://en.wikipedia.org/wiki/Gabor_wavelet, accessed july 2017," 2017 July. [Online]. Available: https://en.wikipedia.org/wiki/Gabor_wavelet,.

[31] T. S. Lee, "Gabor wavelet "Image Representation Using 2D Gabor wavelets"," *IEEE ,* October 1996.

[32] M. U. Akram, S. Khalid, A. Tariq and M. Y. Javeda, "Detection of neovascularization in retinal images using multivariate m-Mediods based classifier," *Computerized Medical Imaging and Graphics,* 2013.

[33] T. K. Sunny Arief Sudiro, "Fingerprint Minutiae Extraction Algorithm using Cross Number on Valley structure," 2007.

[34] "Support Vector Machines," [Online]. Available: https://en.wikipedia.org/wiki/Support_vector_machine. [Accessed July 2018].

[35] [Online]. Available: https://www.analyticsvidhya.com/blog/2017/09/understaing-support-vector-machine-example-code/.